C2	0.20348 (15)	0.3757 (5)	0.0139 (3)	0.0318 (12)
H2	0.2157	0.2965	−0.0018	0.038*
C3	0.16424 (15)	0.3716 (4)	0.0365 (3)	0.0269 (11)
H3	0.1497	0.2885	0.0375	0.032*
C4	0.14579 (14)	0.4876 (4)	0.0578 (3)	0.0197 (10)
C5	0.16748 (15)	0.6093 (4)	0.0566 (3)	0.0257 (11)
H5	0.1549	0.6892	0.0707	0.031*
C6	0.20726 (14)	0.6144 (4)	0.0351 (3)	0.0236 (10)
H6	0.2221	0.6971	0.0347	0.028*
C7	0.07464 (14)	0.4036 (4)	0.0519 (3)	0.0222 (10)
H7	0.0788	0.3410	0.0139	0.027*
C8	0.03340 (13)	0.4058 (4)	0.0765 (2)	0.0168 (9)
C9	−0.00087 (15)	0.3178 (4)	0.0481 (3)	0.0255 (11)
H9	0.0019	0.2505	0.0116	0.031*
C10	−0.03943 (15)	0.3295 (4)	0.0736 (3)	0.0261 (11)
H10	−0.0632	0.2691	0.0560	0.031*
C11	−0.04250 (15)	0.4301 (5)	0.1249 (3)	0.0265 (11)
H11	−0.0687	0.4407	0.1426	0.032*
C12	−0.00710 (14)	0.5167 (4)	0.1508 (3)	0.0223 (10)
H12	−0.0098	0.5870	0.1855	0.027*
C13	0.07108 (15)	0.8261 (4)	0.2653 (2)	0.0236 (10)
C14	0.06750 (18)	0.8781 (5)	0.3451 (3)	0.0326 (12)
C15	0.07746 (15)	0.9195 (4)	0.2105 (3)	0.0249 (11)
H15	0.0810	1.0110	0.2250	0.030*
C16	0.07882 (15)	0.8822 (4)	0.1348 (3)	0.0241 (11)
C17	0.08415 (17)	0.9929 (4)	0.0773 (3)	0.0278 (11)
C18	0.18236 (15)	0.6331 (4)	0.2566 (3)	0.0227 (10)
C19	0.22211 (17)	0.7250 (6)	0.2750 (3)	0.0410 (14)
C20	0.18587 (15)	0.5046 (4)	0.2881 (3)	0.0281 (11)
H20	0.2140	0.4740	0.3162	0.034*
C21	0.14966 (15)	0.4192 (4)	0.2797 (3)	0.0232 (10)
C22	0.15671 (15)	0.2806 (5)	0.3172 (3)	0.0286 (11)
F1	0.11909 (12)	0.9686 (3)	0.0484 (2)	0.0590 (10)
F2	0.04965 (11)	0.9967 (3)	0.01655 (16)	0.0474 (9)
F3	0.08890 (12)	1.1150 (3)	0.10758 (16)	0.0516 (9)
F4	0.03084 (12)	0.8339 (3)	0.3627 (2)	0.0651 (10)
F5	0.06729 (15)	1.0080 (3)	0.35147 (18)	0.0703 (12)
F6	0.09967 (13)	0.8311 (4)	0.40128 (18)	0.0775 (13)
F7	0.22453 (10)	0.8019 (3)	0.2159 (2)	0.0584 (10)
F8	0.21997 (13)	0.8058 (4)	0.3339 (2)	0.0789 (13)
F9	0.26008 (10)	0.6604 (4)	0.2971 (3)	0.0827 (14)
F10	0.13059 (10)	0.2608 (3)	0.3655 (2)	0.0540 (9)
F11	0.19792 (9)	0.2582 (3)	0.35786 (17)	0.0395 (8)
F12	0.14753 (11)	0.1857 (3)	0.26264 (18)	0.0522 (9)

Atomic displacement parameters (Å^2)

	U^{11}	U^{22}	U^{33}	U^{12}	U^{13}	U^{23}

Ni1	0.0209 (3)	0.0193 (3)	0.0168 (3)	−0.0020 (2)	0.0019 (2)	−0.0002 (2)
Br1	0.0284 (3)	0.0261 (3)	0.0550 (4)	−0.0007 (2)	0.0192 (3)	−0.0007 (2)
N1	0.0176 (19)	0.0186 (19)	0.020 (2)	0.0011 (15)	0.0087 (16)	0.0019 (15)
N2	0.019 (2)	0.0198 (18)	0.0171 (19)	0.0022 (15)	0.0002 (16)	0.0014 (15)
O1	0.0265 (17)	0.0234 (17)	0.0181 (16)	−0.0041 (13)	0.0051 (14)	−0.0022 (13)
O2	0.0269 (17)	0.0229 (16)	0.0123 (15)	−0.0012 (13)	0.0052 (14)	0.0002 (12)
O3	0.0202 (17)	0.0289 (17)	0.0248 (17)	−0.0049 (14)	0.0014 (15)	−0.0015 (14)
O4	0.0239 (17)	0.0250 (16)	0.0134 (15)	−0.0003 (13)	0.0001 (14)	0.0030 (13)
C1	0.023 (3)	0.026 (2)	0.028 (3)	0.003 (2)	0.000 (2)	0.001 (2)
C2	0.021 (3)	0.025 (3)	0.055 (4)	0.002 (2)	0.019 (2)	0.000 (2)
C3	0.024 (3)	0.018 (2)	0.041 (3)	−0.0019 (18)	0.013 (2)	0.000 (2)
C4	0.020 (2)	0.020 (2)	0.019 (2)	−0.0013 (18)	0.005 (2)	0.0001 (18)
C5	0.031 (3)	0.023 (2)	0.024 (2)	0.000 (2)	0.008 (2)	−0.002 (2)
C6	0.019 (2)	0.025 (2)	0.032 (3)	−0.0018 (19)	0.016 (2)	0.002 (2)
C7	0.028 (3)	0.016 (2)	0.019 (2)	0.0015 (19)	0.000 (2)	0.0013 (18)
C8	0.016 (2)	0.021 (2)	0.014 (2)	0.0027 (18)	0.0062 (18)	0.0056 (18)
C9	0.030 (3)	0.019 (2)	0.023 (2)	−0.0042 (19)	−0.001 (2)	−0.0012 (19)
C10	0.020 (3)	0.035 (3)	0.023 (3)	−0.008 (2)	0.005 (2)	−0.001 (2)
C11	0.023 (3)	0.038 (3)	0.020 (2)	−0.001 (2)	0.007 (2)	0.002 (2)
C12	0.022 (3)	0.027 (2)	0.017 (2)	0.0056 (19)	0.003 (2)	0.0011 (18)
C13	0.029 (3)	0.024 (2)	0.017 (2)	−0.005 (2)	0.003 (2)	−0.0033 (19)
C14	0.049 (3)	0.027 (3)	0.024 (3)	−0.012 (2)	0.012 (3)	−0.005 (2)
C15	0.031 (3)	0.020 (2)	0.025 (3)	−0.0018 (19)	0.009 (2)	−0.0032 (19)
C16	0.025 (3)	0.019 (2)	0.023 (2)	−0.0035 (18)	−0.003 (2)	0.0025 (19)
C17	0.034 (3)	0.024 (2)	0.026 (3)	−0.001 (2)	0.009 (2)	0.001 (2)
C18	0.025 (3)	0.029 (3)	0.015 (2)	−0.005 (2)	0.007 (2)	−0.0012 (19)
C19	0.030 (3)	0.044 (3)	0.046 (4)	−0.011 (3)	0.003 (3)	0.005 (3)
C20	0.020 (2)	0.034 (3)	0.027 (3)	0.001 (2)	0.000 (2)	0.002 (2)
C21	0.026 (3)	0.026 (2)	0.016 (2)	0.002 (2)	0.002 (2)	−0.0045 (19)
C22	0.023 (3)	0.033 (3)	0.030 (3)	0.001 (2)	0.008 (2)	0.003 (2)
F1	0.064 (2)	0.051 (2)	0.075 (3)	0.0070 (17)	0.042 (2)	0.0280 (18)
F2	0.059 (2)	0.0475 (19)	0.0271 (16)	−0.0053 (15)	−0.0060 (16)	0.0152 (14)
F3	0.100 (3)	0.0219 (15)	0.0304 (17)	−0.0123 (16)	0.0116 (18)	0.0018 (13)
F4	0.077 (3)	0.076 (2)	0.058 (2)	−0.030 (2)	0.045 (2)	−0.0352 (19)
F5	0.158 (4)	0.0290 (18)	0.0383 (19)	−0.0167 (19)	0.052 (2)	−0.0129 (14)
F6	0.086 (3)	0.113 (3)	0.0216 (17)	0.031 (2)	−0.0094 (19)	−0.0215 (19)
F7	0.050 (2)	0.066 (2)	0.056 (2)	−0.0321 (17)	0.0068 (18)	0.0199 (18)
F8	0.081 (3)	0.090 (3)	0.069 (3)	−0.051 (2)	0.022 (2)	−0.045 (2)
F9	0.0247 (18)	0.076 (3)	0.136 (4)	−0.0113 (18)	−0.004 (2)	0.041 (3)
F10	0.046 (2)	0.054 (2)	0.072 (2)	0.0198 (15)	0.0331 (19)	0.0345 (17)
F11	0.0330 (16)	0.0378 (16)	0.0419 (18)	0.0070 (13)	−0.0021 (15)	0.0108 (13)
F12	0.068 (2)	0.0274 (16)	0.050 (2)	0.0015 (15)	−0.0074 (18)	−0.0033 (15)

Geometric parameters (Å, °)

Ni1—O3	2.020 (3)	C9—H9	0.9500
Ni1—O4	2.044 (3)	C10—C11	1.372 (6)
Ni1—O2	2.045 (3)	C10—H10	0.9500
Ni1—N2	2.063 (3)	C11—C12	1.393 (6)

Ni1—O1	2.066 (3)	C11—H11	0.9500
Ni1—N1	2.113 (4)	C12—H12	0.9500
Br1—C1	1.897 (5)	C13—C15	1.394 (6)
N1—C7	1.291 (5)	C13—C14	1.531 (7)
N1—C4	1.426 (6)	C14—F5	1.304 (5)
N2—C12	1.332 (6)	C14—F6	1.317 (6)
N2—C8	1.358 (5)	C14—F4	1.332 (6)
O1—C13	1.258 (5)	C15—C16	1.399 (6)
O2—C16	1.255 (5)	C15—H15	0.9500
O3—C18	1.253 (5)	C16—C17	1.538 (6)
O4—C21	1.265 (5)	C17—F2	1.326 (5)
C1—C6	1.376 (6)	C17—F3	1.327 (5)
C1—C2	1.393 (6)	C17—F1	1.334 (6)
C2—C3	1.379 (6)	C18—C20	1.394 (6)
C2—H2	0.9500	C18—C19	1.517 (7)
C3—C4	1.388 (6)	C19—F7	1.313 (6)
C3—H3	0.9500	C19—F9	1.325 (6)
C4—C5	1.396 (6)	C19—F8	1.331 (7)
C5—C6	1.386 (6)	C20—C21	1.397 (6)
C5—H5	0.9500	C20—H20	0.9500
C6—H6	0.9500	C21—C22	1.529 (6)
C7—C8	1.456 (6)	C22—F10	1.330 (6)
C7—H7	0.9500	C22—F12	1.333 (5)
C8—C9	1.384 (6)	C22—F11	1.333 (5)
C9—C10	1.390 (7)		
O3—Ni1—O4	89.27 (12)	C11—C10—C9	118.7 (4)
O3—Ni1—O2	84.55 (12)	C11—C10—H10	120.7
O4—Ni1—O2	173.82 (12)	C9—C10—H10	120.7
O3—Ni1—N2	177.27 (13)	C10—C11—C12	119.8 (5)
O4—Ni1—N2	89.36 (12)	C10—C11—H11	120.1
O2—Ni1—N2	96.80 (12)	C12—C11—H11	120.1
O3—Ni1—O1	87.79 (12)	N2—C12—C11	121.9 (4)
O4—Ni1—O1	91.93 (12)	N2—C12—H12	119.1
O2—Ni1—O1	87.99 (12)	C11—C12—H12	119.1
N2—Ni1—O1	94.62 (13)	O1—C13—C15	128.3 (4)
O3—Ni1—N1	98.24 (13)	O1—C13—C14	114.1 (4)
O4—Ni1—N1	87.91 (12)	C15—C13—C14	117.7 (4)
O2—Ni1—N1	92.82 (12)	F5—C14—F6	108.1 (4)
N2—Ni1—N1	79.35 (14)	F5—C14—F4	106.8 (5)
O1—Ni1—N1	173.97 (13)	F6—C14—F4	104.4 (4)
C7—N1—C4	120.1 (4)	F5—C14—C13	114.9 (4)
C7—N1—Ni1	111.8 (3)	F6—C14—C13	111.0 (4)
C4—N1—Ni1	127.9 (3)	F4—C14—C13	111.0 (4)
C12—N2—C8	118.6 (4)	C13—C15—C16	121.8 (4)
C12—N2—Ni1	127.8 (3)	C13—C15—H15	119.1
C8—N2—Ni1	113.2 (3)	C16—C15—H15	119.1
C13—O1—Ni1	121.6 (3)	O2—C16—C15	129.0 (4)
C16—O2—Ni1	121.2 (3)	O2—C16—C17	112.9 (4)
C18—O3—Ni1	126.3 (3)	C15—C16—C17	118.1 (4)

C21—O4—Ni1	124.0 (3)	F2—C17—F3	106.8 (4)
C6—C1—C2	121.5 (5)	F2—C17—F1	106.0 (4)
C6—C1—Br1	119.2 (3)	F3—C17—F1	107.4 (4)
C2—C1—Br1	119.2 (3)	F2—C17—C16	111.0 (4)
C3—C2—C1	118.9 (4)	F3—C17—C16	114.7 (4)
C3—C2—H2	120.5	F1—C17—C16	110.5 (4)
C1—C2—H2	120.5	O3—C18—C20	127.6 (4)
C2—C3—C4	120.7 (4)	O3—C18—C19	112.9 (4)
C2—C3—H3	119.7	C20—C18—C19	119.5 (4)
C4—C3—H3	119.7	F7—C19—F9	107.5 (5)
C3—C4—C5	119.4 (4)	F7—C19—F8	106.8 (5)
C3—C4—N1	122.4 (4)	F9—C19—F8	106.1 (5)
C5—C4—N1	118.2 (4)	F7—C19—C18	112.7 (4)
C6—C5—C4	120.5 (4)	F9—C19—C18	113.3 (4)
C6—C5—H5	119.8	F8—C19—C18	110.0 (5)
C4—C5—H5	119.8	C18—C20—C21	122.6 (4)
C1—C6—C5	119.0 (4)	C18—C20—H20	118.7
C1—C6—H6	120.5	C21—C20—H20	118.7
C5—C6—H6	120.5	O4—C21—C20	128.4 (4)
N1—C7—C8	119.5 (4)	O4—C21—C22	112.9 (4)
N1—C7—H7	120.3	C20—C21—C22	118.7 (4)
C8—C7—H7	120.3	F10—C22—F12	107.4 (4)
N2—C8—C9	122.1 (4)	F10—C22—F11	107.0 (4)
N2—C8—C7	114.9 (4)	F12—C22—F11	106.3 (4)
C9—C8—C7	123.0 (4)	F10—C22—C21	111.5 (4)
C8—C9—C10	119.0 (4)	F12—C22—C21	110.5 (4)
C8—C9—H9	120.5	F11—C22—C21	113.9 (4)
C10—C9—H9	120.5		

Fig. 1

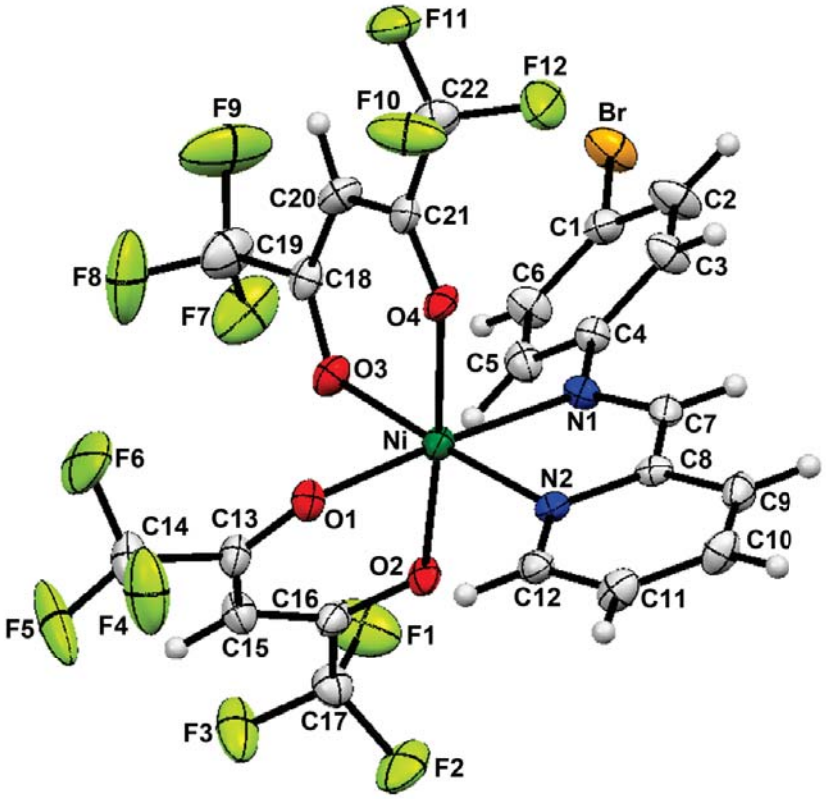
F11
F12
C22
F10
F9
Br
C20
C21
C2
C1
C19
C3
F8
C18
C6
F7
O4
C4
O3
C5
N1
C7
Ni
F6
C8
N2
C9
C14
C13
O1
C10
O2
C12
C11
C16
F5
F4
F1
C15
C17
F3
F2

Fig. 2

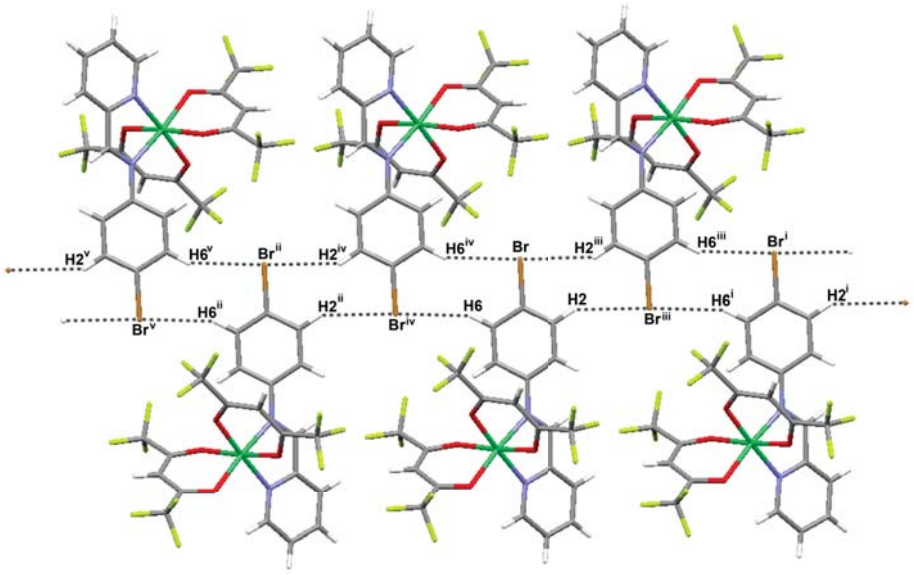
H2v
H6v
Brii
H2iv
H6iv
Br
H2iii
H6iii
Bri
Brv
H6ii
H2ii
Briv
H6
H2
Briii
H6i
H2i

Fig. 3

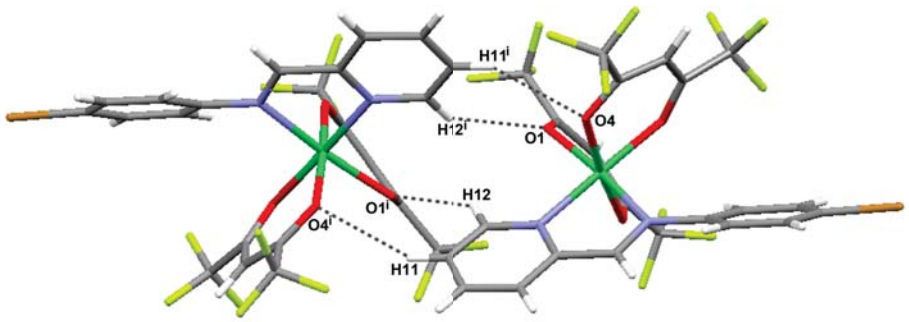

Appendix Four

Manuscript II

Redox Coupled-Spin Crossover in Cobalt β-Diketonate Complexes: Observation of the High Spin Co^{III} Intermediate

*Phimphaka Harding,**[a] *David J. Harding,**[a] *Rattawat Daengngern,*[a] *Theeraphol Thurakitsaree,*[b] *Brian M. Schutte,*[c] *Michael J. Shaw*[c] and *Yuthana Tantirungrotechai*[d]

Molecular Technology Research Unit, School of Science, Walailak University, Thasala, Nakhon Si Thammarat, 80161, Thailand.

E-mail: kphimpha@wu.ac.th or hdavid@wu.ac.th

RECEIVED DATE (to be automatically inserted after your manuscript is accepted if required according to the journal that you are submitting your paper to)

TITLE RUNNING HEAD 'Redox-Coupled Spin Crossover in $[Co(\beta\text{-diketonate})_2(N\text{-}N)]^{0/+}$ Complexes'

[a] Molecular Technology Research Unit, School of Science, Walailak University, Thasala, Nakhon Si Thammarat, 80161, Thailand, [b] Department of Physics, Faculty of Science, Chiang Mai University, Chiang Mai, 50200, Thailand, [c] Box 1652, Department of Chemistry, Southern Illinois University Edwardsville, IL, USA, [d] National Nanotechnology Center, National Science and Development Agency, Pathumthani, 12120, Thailand

ABSTRACT

Electrochemical, spectroelectrochemical, magnetic and spectroscopic properties are reported for the octahedral cobalt β-diketonate complexes, $[Co(\beta\text{-diketonate})_2(N\text{-}N)]$ {β-diketonate = 2,2,6,6-tetramethylheptane-3,5-dionate (tmhd); N-N = 1,10-phenanthroline (phen) **1**, 2,2′-bipyridine (2,2′-bpy) **2** and dimethylaminoethylamine (dmae) **3**; β-diketonate = 1,3-diphenylpropane-1,3-dionate (dbm); N-N =

phen **4**, 2,2′-bpy **5**, dmae **6**}. Cyclic voltammetry of **1**-**6** reveals an irreversible one-electron oxidation to Co^{III} with large peak separations between the oxidation and reduction peaks, indicative of redox coupled-spin crossover (RCSCO); i.e. [Co(β-diketonate)$_2$(N-N)] (S = 3/2) ↔ [Co(β-diketonate)$_2$(N-N)]$^+$ + e^- (S = 0). Notably, the high spin Co^{III} intermediate has been observed electrochemically for the *first time*. Moreover, the complexes represent rare examples of RCSCO species with a CoO_4N_2 coordination sphere. The tmhd complexes are more easily oxidized than the respective dbm analogues with the oxidation peak potentials in the order bipy < phen < dmae. Oxidation of **1**-**6** with $AgBF_4$ yields the corresponding Co^{III} cations, [Co(β-diketonate)$_2$(N-N)]BF_4 **1**$^+$-**6**$^+$ which has been confirmed by ^{1}H NMR spectroscopy. Spectroelectrochemistry of the redox pairs [Co(β-diketonate)$_2$(N-N)]$^{0/+}$ is consistent with the isolated compounds being identical to the species formed at the electrode. Theoretical studies reveal that the SOMO is essentially metal *d*-orbital and β-diketonate based, consistent with the strong effect of the β-diketonate ligand on the oxidation potential. In addition, there are substantial changes in the relative stabilities of the various spin states compared with [Co(tacn)$_2$]$^{2+/3+}$ such that the high spin states become more accessible. The above results are consistent with a square scheme mechanism in which oxidation and reduction proceeds through high spin Co^{III} and low spin Co^{II} intermediates, respectively.

Introduction

Spin crossover is one of the most interesting and widely studied phenomena of transition metal complexes in part due to the possible applications of such complexes in fields such as molecular electronics, memory storage and display devices.[1-4] In principle, a coordination complex with any electron configuration from d^4-d^7 may exhibit spin crossover but the most extensively studied systems are those of d^6 Fe^{II}.[5-14] In addition, in most reported cases the iron center is surrounded by six nitrogen donors as this provides the intermediate ligand field required for spin crossover (e.g. [Fe(phen)$_2$(NCS)$_2$]).[15] Unlike Fe^{II}, spin crossover in cobalt(II) complexes is rather rare with [Co(bipy)$_3$]$^{2+}$ and [Co(terpy)$_2$]$^{2+}$ as perhaps the best known examples.[16-19]

While spin crossover systems have been widely studied, comparatively little attention has been given to reactions in which the spin crossover is coupled to electron transfer. This situation is surprising given that reactions in which electron transfer is accompanied by a change in spin state are widespread in both chemistry and biology.[2-4,20-23] For instance in cytochrome P450, substrate binding produces a change in spin state of the Fe^{III} heme active site thereby shifting the redox potential and triggering an electron transfer which initiates the catalytic cycle of the enzyme.[24,25] Further examples include the iron-molybdenum cofactor of nitrogenase and cytochrome *c* peroxidases.[26-28] In relation to coordination chemistry the oxidation of high spin (HS) Co^{II} to low spin (LS) Co^{III} is a well known example of redox

coupled-spin crossover (RCSCO).[29] As with the spin crossover complexes discussed earlier most complexes exhibiting RCSCO have N_6 coordination environments. Furthermore, although the mechanism of such reactions has been debated for many years it is still unclear whether the reaction proceeds in a concerted fashion or via higher energy spin state intermediates.[30-37] However, recently Schultz and co-workers have shown that the reduction of $[Co(tacn)_2]^{3+}$ (tacn = 1,4,7-triazacyclononane) appears to proceed through a high spin Co^{III} intermediate.[38-40]

In this paper we report the synthesis of a series of octahedral cobalt β-diketonate complexes, [Co(β-diketonate)$_2$(N-N)] {β-diketonate = 2,2,6,6-tetramethylheptane-3,5-dionate (tmhd); N-N = 1,10-phenanthroline (phen) **1**, 2,2′-bipyridine (2,2′-bpy) **2** and dimethylaminoethylamine (dmae) **3**; β-diketonate = 1,3-diphenylpropane-1,3-dionate (dbm); N-N = phen **4**, 2,2′-bpy **5**, dmae **6**} which are shown to undergo redox coupled-spin crossover. Oxidation of these complexes yields the low spin d^6 Co^{III} cations $[Co(\beta\text{-diketonate})_2(N\text{-}N)]^+$. Electrochemical studies show the presence of the HS Co^{III} intermediate, a first for any RCSCO system. Moreover, unusually for redox coupled-spin crossover species the complexes possess a CoN_2O_4 coordination sphere rather than the more common CoN_6 coordination environment. Finally, through computational studies we attempt to rationalize the observed behavior in these complexes.

Results and Discussion

Synthesis of [Co(β-diketonate)$_2$(N-N)]. Reaction of $[Co(tmhd)_2(H_2O)_2]$ or $[Co(dbm)_2(H_2O)_2]$ (tmhd = 2,2,6,6-tetramethylheptane-3,5-dionate, dbm = 1,3-diphenylpropane-1,3-dionate) and N-N donor ligands in THF or CH_2Cl_2 yields the Co^{II} complexes [Co(β-diketonate)$_2$(N-N)] {β-diketonate = tmhd; N-N = 1,10-phenanthroline (phen) **1**, 2,2′-bipyridine (2,2′-bpy) **2** and dimethylaminoethylamine (dmae) **3**; β-diketonate = dbm; N-N = phen **4**, 2,2′-bpy **5**, dmae **6**; Scheme 1}. The complexes are orange and air stable. IR spectroscopy of **1**-**6** shows the ν_{CO} band between 1583 and 1595 cm^{-1} indicating that the β-diketonate ligands adopt a chelating coordination mode (Table 1).[41] Similar bands have been observed in the related Ni analogues which are observed between 1582 and 1595 cm^{-1}.[42] The two dmae complexes, **3** and **6**, also exhibit ν_{NH} bands at 3362 and 3365 cm^{-1}, respectively, and are again almost identical with those of their Ni counterparts. Magnetic susceptibility measurements indicate that the complexes are paramagnetic with μ_{eff} between 4.41 and 5.03 BM consistent with high spin Co^{II}.[43]

UV-Vis spectroscopy of the compounds in CH_2Cl_2 supports an octahedral Co^{II} coordination environment with a low intensity band at *ca*. 570 nm which by comparison with $[Co(hfac)_2(tmeda)]$ (hfac = hexafluoroacetylacetonate) is assigned to an overlap between the $^4T_{1g}$ (F) → $^4T_{2g}$ (P) and $^4T_{1g}$ (F) → $^4A_{2g}$ (F) transitions.[44] Additional, very intense bands are found in the UV region which are

ascribed to ligand centered $\pi \rightarrow \pi^*$ transitions.[45] Similar bands are observed for other [Co(β-diketonate)$_2$(N-N)] (β-diketonate = acac, hfac; N-N = en, 2,2′-bipy, phen) complexes.[46,47]

Synthesis of [Co(β-diketonate)$_2$(N-N)]$^+$. The peak potentials from the electrochemical studies suggested that oxidation of the neutral complexes could be achieved with Ag^+ (*vide infra*). Thus, addition of one equivalent of $AgBF_4$ to the isolated Co^{II} species affords the cationic complexes [Co(tmhd)$_2$(N-N)][BF_4] (N-N = phen **1**$^+$, 2,2′-bpy **2**$^+$ and dmae **3**$^+$) and [Co(dbm)$_2$(N-N)][BF_4] (N-N = phen **4**$^+$, 2,2′-bpy **5**$^+$ and dmae **6**$^+$) as green-brown or purple compounds (Table 3). They may also be prepared in a stepwise, one pot reaction from [Co(β-diketonate)$_2$(H_2O)$_2$] followed by addition of the appropriate ligand and subsequent addition of $AgBF_4$ giving **1**$^+$-**6**$^+$. The ν_{CO} of **1**$^+$-**6**$^+$ shift to lower wavenumbers by *ca.* 40 or 70 cm^{-1} for the tmhd and dbm complexes respectively. Related [Co(acac)$_2$(N-N)]$^+$ (N-N = 2,2′-bpy, en) complexes show ν_{CO} bands at 1524 and 1528 cm^{-1} confirming that the Co^{III} complexes have been formed.[48-50]

The cationic complexes despite their different colors exhibit very similar electronic spectra to **1**-**6** with a band at *ca.* 550 nm which by comparison with [Co(acac)$_2$(N-N)]$^+$ (N-N = en, bipy, phen) is assigned to the $^1A_{1g}$ (F) $\rightarrow$ $^1T_{1g}$ transition.[48-50] As with the neutral complexes additional charge transfer transitions are evident below 350 nm. The band at *ca.* 290 nm for **1**$^+$, **2**$^+$, **4**$^+$ and **5**$^+$, is assigned to an MLCT transition while the other bands are assigned to β-diketonate $\pi \rightarrow \pi^*$ transitions.[48]

NMR Spectroscopy. The ^{1}H NMR spectra of **1**$^+$-**6**$^+$ show sharp, readily identifiable peaks consistent with a low spin d^6 electron configuration (Table 3). The ^{1}H NMR spectra of **1**$^+$, **2**$^+$, **4**$^+$ and **5**$^+$ show signals in the aromatic region consistent with the presence of coordinated phen and bipy ligands and are assigned on the basis of coupling constants, integration values and comparison with the related [Co(acac)$_2$(N-N)]$^+$ (N- N = bipy and phen) complexes.[48, 49] As expected we observe a single resonance for the central β-diketonate proton indicating that the β-diketonate ligands are magnetically equivalent. In the case of **1**$^+$ and **2**$^+$ there are two singlets between 1.32-0.80 ppm for the *t*-butyl groups. The phenyl protons for the dbm ligands in **4**$^+$ and **5**$^+$ are observed between 6.97-8.04 ppm as a series of multiplets.

The dmae complexes show more complex spectra as a result of the asymmetry of the dmae ligand. This is most clearly evidenced by the presence of two singlets for the β-diketonate hydrogen confirming the magnetic inequivalence of the β-diketonate ligands. Moreover, in the case of **3**$^+$ there are three resonances for the *t*-butyl groups integrating in a ratio of 2:1:1 indicating that two of the singlets are coincident. As with **4**$^+$ and **5**$^+$, the phenyl protons for the dbm ligands of **6**$^+$ are split into a number of doublets and multiplets between 7.37 and 8.10 ppm. The dmae ligands show two sharp singlets for the

methyl groups but four broad resonances for the individual protons on the ligand's backbone. The amino protons are not observed in both cases possibly due to H-bonding.[42]

Electrochemistry. The complexes **1**-**6** have been studied by cyclic voltammetry (CV) and square wave voltammetry in dry CH_2Cl_2 under anaerobic conditions and reveal irreversible one-electron oxidation. The CV of $[Co(tmhd)_2(phen)]$ is shown in Figure 1a as a representative example. The cyclic voltammograms (CVs) are broadly similar, exhibiting a single oxidation peak, Epa_1, and in most cases a small reduction peak, Epc_1, followed by a much larger reduction peak, Epc_2, which is widely separated from Epa_1 (Table 2). The irreversibility of the redox processes, which contrast with the Ni analogues which show either quasi-reversible oxidation or completely chemically irreversible oxidations with no corresponding reduction peaks,[42] suggests that the oxidation/reduction is accompanied by a structural and electronic rearrangement. Thus the oxidation of **1-6** to Co^{III} (Epa_1) initially produces a high spin Co^{III} intermediate (Epc_1) which can be re-reduced close to the oxidation peak, Epa_1. Epc_1 is presumably the cathodic partner to the anodic peak represented by Epa_1 and is to the best of our knowledge the *first time the HS Co^{III} intermediate has been observed electrochemically in a redox coupled-spin crossover system*. The high spin Co^{III} species rapidly undergoes spin crossover to the more stable low spin Co^{III} isomer which is reduced at a significantly more negative potential (Epc_2) resulting in a wide separation between the oxidation and reduction peak potentials, Epa_1 and Epc_2. The redox behavior of these complexes is an example of *redox coupled-spin crossover*.[51,52] This behavior is best described by the square scheme shown in Scheme 2. The two processes *1* and *3* represent the oxidation and reduction reactions of the individual spin state isomers while processes *2* and *4* represent the spin exchange reactions in the individual oxidation states.. Redox coupled-spin crossover has also been observed and extensively studied by Schultz *et al*. in a series of $[M(tacn)_2]^{2+/3+}$ (M = Fe, Co; tacn = 1,4,7-triazacyclononane) complexes although in this system the redox processes are fully reversible.[38-40] Similar redox behavior to **1**-**6** has recently been reported in the dimeric complex $[(bpbp)Co_2(O_2P(OPh)_2)_2]^+$ ($bpbp^-$ = 2,6-bis(N,N′-bis-(2-picolyl)amino)methyl)-4-tertbutylphenolato) which also shows wide separation of the oxidation and reduction peaks.[53] A similar result is also found in the case of $[(Tp^R)_2Co]^{0/+}$ (Tp^R = Tp, pzTp and Tp*) where increasing steric bulk results in a corresponding increase in irreversibility.[54] Comparisons between $[Co(tacn)_2]^{2+}$ and complexes **1**-**6** show that the former is oxidized *ca*. 0.9 V more easily than the latter consistent with the greater stability of the Co^{II} oxidation state for the $[Co(\beta\text{-diketonate})_2(N\text{-}N)]$ complexes. In contrast, the $[(bpbp)Co_2(O_2P(OPh)_2)_2]^+$ dimer oxidizes at a higher potential, 0.42 V (vs. $[FeCp_2]^{0/+}$).

The oxidation peak potentials for **1**-**6** are ca. 0.54 V more negative than the related Ni compounds.[42] A similar difference in the redox potentials has also been observed in the two series $[M(tacn)_2]^{2+/3+}$ and $[(Tp^R)_2M]^{0/+}$ (Tp^R = Tp, pzTp and Tp*; M = Co, Ni).[38,54-56] Within the two series of

1-**6** we find that the tmhd complexes are easier to oxidize than the corresponding dbm complexes by *ca*. 0.14 V indicating that the inductive effects of the *t*-butyl groups increase the electron density on the metal thereby making it easier to oxidize. A similar trend is observed for the Ni analogues although the difference is larger by ca. 0.30 V.[42] The Co complexes show oxidation peak potentials in the order bipy < phen < dmae. This order is surprising given that for the [Ni(β-diketonate)$_2$(N-N)] complexes the dmae compounds are the most easily oxidized which is more in line with the typical electron donating properties of diamine and diimine ligands. The difference in the order of the peak potentials may be the result of the spin change which occurs upon oxidation. The difference in the oxidation and reduction peak potentials ($\Delta E = Epa_1$-Epc_2) varies from 0.54-1.06 V with **1**-**3** exhibiting larger ΔE values than **4**-**6**, thereby indicating that the greater steric bulk of the *t*-butyl groups results in a reduction in the rate of electron-transfer. Similar observations in the $[(Tp^R)_2Co]^{0/+}$ series are also attributed to steric effects.[54] In the case of $[(bpbp)Co_2(O_2P(OPh)_2)_2]^+$ ΔE = 1.04 and 0.61 V for the two redox reactions which agrees well with our findings for **1**-**6**.[53]

It is interesting to note that while the $[Co(tacn)_2]^{2+/3+}$ and $[(Tp^R)_2Co]^{0/+}$ redox pairs have a CoN_6 coordination sphere **1**-**6** and $[(bpbp)Co_2(O_2P(OPh)_2)_2]^+$ possess CoN_2O_4 and CoN_3O_3 coordination spheres, respectively. The presence of the weaker field oxygen donors would be expected to favor the high spin isomers and may be responsible for the irreversibility seen in these systems. It may also explain why we are able to observe a reduction peak for the high spin Co^{III} intermediate in some of the complexes.

In an attempt to better understand the redox coupled-spin crossover process in complexes **1**-**6** we undertook cyclic voltammetric studies at high scan rates using a microelectrode. There was little change in the reversibility of the complexes even at moderately fast scan rates (10 Vs^{-1}) consistent with a rapid spin exchange equilibrium and slow electron transfer as is frequently observed in these systems (Figure 2).[29,52] This result seems reasonable since going from the high spin to the low spin state does not require any bonds to be broken but rather optimization of the Co-ligand bond lengths. Similar irreversibility at high scans rates is also observed in the $[(bpbp)Co_2(O_2P(OPh)_2)_2]^+$ dimer. In addition, studies on a wide range of cobalt am(m)ine systems also reveal slow electron transfer.[52]

Despite the fact that redox coupled-spin crossover reactions are well documented the mechanism still remains the subject of considerable debate with a pathway via high energy spin-state intermediates and a concerted pathway both proposed.[30-37] Schultz and co-workers have shown that in the case of the $[Co(tacn)_2]^{2+/3+}$ redox pair the reaction proceeds via a high-spin intermediate.[39,40] As noted earlier the cyclic voltammograms of **1**-**6** clearly show the presence of peaks attributable to a high spin Co^{III} intermediate and suggest that the mechanism for the oxidation of **1**-**6** also proceeds via a high spin intermediate. In contrast, at all applied scan rates (0.02 to 10 Vs^{-1}) we were unable observe a peak for

the low spin Co^{II} intermediate suggesting that the lifetime of this intermediate is very short as a result of an exceedingly rapid spin exchange reaction (equilibrium *4* in Scheme 2).

The square wave voltammograms show peak potentials similar to those found in the CVs. The slight deviations between the two methods might be due to the dependence of the peak potentials on scan rate noted in the CVs. The peaks also exhibit slight asymmetry consistent with the electrochemical irreversibility observed in the CVs.

The cations $\mathbf{1}^{+}$-$\mathbf{6}^{+}$ were also studied by cyclic voltammetry and show a large reduction peak coupled to a smaller redox couple at a higher potential (Figure 1-b). The peak potentials observed in the cyclic voltammograms are almost identical to those found in the neutral analogues although there are slight deviations. Similar results are noted in the complex $[(bpbp)Co_2(O_2P(OPh)_2)_2]^{3+}$ where shifts of up to 0.18 V are observed.[53] As with **1**-**6** the peaks for the high spin Co^{III} intermediate are clearly discernable but no peak is apparent (i.e. "Epa_2") for the low spin Co^{II} intermediate. Such behavior is typical of square scheme systems which involve first order isomerization of an initial electrode product to the final observed form.[57] Furthermore, the apparent reversibility of the CV's do not change with concentration a result which rules out significant contribution of the second-order homogeneous cross reaction (i.e. LS Co^{II} + HS Co^{III} → LS Co^{III} + HS Co^{II}) to the observed current.[57] In such a reaction, the HS Co^{III} produced by equilibrium *2* in Scheme 2 would react with electrogenerated LS Co^{II}. Thus, the reduction of the LS Co^{III} to HS Co^{II} proceeds by the expected LS Co^{II} intermediate. Similar reasoning leads to the conclusion that the oxidation of the HS Co^{II} to LS Co^{III} proceeds by the observed HS Co^{III} intermediate.

To confirm that the products isolated from the chemical oxidation of **1**-**6** were the same as those observed in the cyclic voltammograms we undertook IR spectroelectrochemical studies. The results are detailed in Table 4 with a representative difference spectrum shown in Figure 3. The oxidation of **1**-**6** are all accompanied by the loss (i.e. downward-pointing features) of the β-diketonate ν_{CO} bands at *ca*. 1590, 1570, 1520 and 1500 cm^{-1} due to the Co^{II} starting materials and a corresponding increase in bands at between *ca*. 1550 and 1520 cm^{-1} due to the Co^{III} products. Bands at frequencies lower than 1500 cm^{-1} are lost due to interference from the electrolyte. Subsequent reduction restores the original spectrum showing (as expected) that the chemical oxidation or reduction is reversible. The shift in the bands to lower wavenumbers mirrors exactly what is observed in the isolated complexes and is consistent with the higher Co^{III} oxidation state. Moreover, the positions of the bands are almost identical between the isolated redox pairs and the results from spectroelectrochemistry confirm that the isolated complexes are the species formed at the electrode. Similar studies on the cationic species $\mathbf{1}^{+}$-$\mathbf{6}^{+}$ show an exact opposite trend with bands moving to higher wavenumbers as one would expect. Consistent with the CV results,

no features due to HS Co^{III} were observed, consistent with the presence of a very small equilibrium concentration.

Computational Studies. In order to better understand the electronic structure of **1**-**6**, and their respective cations, and in particular the role of the electronic structure on the redox coupled-spin crossover process we have undertaken DFT calculations.[58] For a given complex, all possible spin states were considered.

The fact that $[Co(dbm)_2(phen)]$ (**4**) has been structurally characterized by single crystal X-ray crystallography allows a comparison between the computational and experimental geometries (see Figure 4 and Table 5).[59] The computed bond lengths match well with the experimental bond lengths with differences no more than 0.05 Å. The bonds angles show similar agreement between experiment and theory. Good agreements between the X-ray structure and computed geometry of $[Co(dbm)_2(phen)]$ in the quartet spin state indicates that these complex exists in a high spin state. It also confirms that the B3LYP/SDD model can be used to describe these types of complexes.

Our B3LYP/SDD calculations confirm the observation that the HS state is the most stable state for the Co^{II} complexes and the LS state is the most stable state for the Co^{III} complexes and as such is consistent the magnetic susceptibility measurements. In contrast, with the previously studied $[Co(tacn)_2]^{2+/3+}$ redox pair the gas-phase energy difference between the HS and LS states, E(HS)-E(LS), for the neutral Co^{II} complexes is between -12.7 and -15.6 kcal/mol (see Table 6) compared with -0.09 kcal/mol for $[Co(tacn)_2]^{2+}$. However, in the case of the Co^{III} cations the gap is significantly decreased to between 16.1 and 18.1 kcal/mol (*cf.* 45.3 kcal/mol for $[Co(tacn)_2]^{3+}$). Judging from the gas-phase energy, the triplet and quintet states are found to lie close to each other. The differences between E(HS)-E(LS) of $\mathbf{1}^+$-$\mathbf{6}^+$ and $[Co(tacn)_2]^{3+}$ are simply explained by the presence of the lower field β-diketonate ligands which are better able to stabilize the HS states. The thmd ligand stabilizes the HS state compared to the LS state to a greater extent than the dbm ligand. Moreover, the phen ligand stabilizes the HS state most in comparison with the other N-N ligands. This might be due to a d-π∗ orbital interaction from the low-lying π∗ orbital of the phen ligand. The smaller difference in the LS and HS states in $\mathbf{1}^+$-$\mathbf{6}^+$ might also explain why we are able to observe the reduction peak for the HS Co^{III} species in some of the electrochemical studies. These studies further suggest that the mechanism for the redox coupled-spin crossover involves a HS Co^{III} intermediate as has also been found in the $[Co(tacn)_2]^{2+/3+}$ system.

The molecular orbital analysis reveals that in the case of **1**-**3** and **6** complexes the SOMO is composed of an antibonding interaction between β-diketonate oxygen *p*-orbitals and the cobalt d_{z2} orbital (see Figure 5). The dmae complexes also exhibit an additional antibonding interaction between

the metal orbital and a hybrid σ donor orbital on the NMe_2 nitrogen of the dmae ligand. The SOMO of related bipy and phen complexes, **4** and **5** are different from the others with a metal d_{xz} orbital involved in a weaker antibonding interaction with the β-diketonate ligands. The significant electron density on the β-diketonate ligands in **1**-**6** is consistent with the strong influence of the β-diketonate upon the oxidation potentials of the above complexes. In the case of **1**, **2**, **4** and **5** the LUMO is essentially a low lying phen or bipy π* orbital while for **3** and **6** the absence of such π* orbitals results in a LUMO which is dominated by a β-diketonate π* orbital (Figure 6). Consequently, a much larger SOMO-LUMO gap is observed in the case of the dmae complexes compared with **1**, **2**, **4** and **5** (see Table 6).

Conclusions. In summary, six redox-active Co β-diketonate complexes have been prepared in two oxidation states which undergo a rare redox coupled-spin crossover from high spin d^7 to low spin d^6 which has been confirmed by cyclic voltammetry and spectroelectrochemical studies. Chemical oxidation of the Co β-diketonate compounds permits isolation of the Co^{III} cations which are indeed low spin as shown by NMR spectroscopy. Electrochemical and computational studies on the redox pairs strongly suggest that the redox coupled-spin crossover in the above complexes proceeds via a square scheme mechanism which does not involve significant amount of homogenous cross-reaction.

Experimental Section

Materials. All reactions were conducted in air using HPLC grade solvents. $[Co(tmhd)_2(H_2O)_2]$, and $[Co(dbm)_2(H_2O)_2]$ were prepared by literature methods.[60,61] All other chemicals were purchased from Fluka Chemical Company and used as received. Elemental analyses and ESI-MS were carried out by the staff of the School of Chemistry, University of Bristol, UK. Elemental analyses were carried out on a Eurovector EA3000 analyser. ESI-MS were carried out on a Bruker Daltonics 7.0T Apex 4 FTICR Mass Spectrometer. Magnetic susceptibilities were determined using the Evan's method at 297 K.[62]

Spectroscopy. Infrared spectra, as KBr discs, were recorded on a Perkin-Elmer Spectrum One infrared spectrophotometer in the range 400-4000 cm^{-1}. Electronic spectra were recorded in CH_2Cl_2 on a Unicam UV300 UV-Visible spectrometer. ^1H NMR spectra were recorded on a Bruker 300 MHz FT-NMR spectrometer at 298 K in $CDCl_3$ with $SiMe_4$ added as an internal standard.

Electrochemistry. Electrochemical studies were carried out using a palmsensPC Vs 2.11 potentiostat in conjunction with a three electrode cell. The auxiliary electrode was a platinum rod and the working electrode was a platinum disc (2.0 mm diameter). The reference electrode was a Ag-AgCl electrode. Solutions were 5 x 10^{-4} M in the test compound and 0.1 M in $[NBu^n_4][PF_6]$ as the supporting electrolyte. Under these conditions, $E^{o\prime}$ for the one-electron oxidation of $[Fe(\eta\text{-}C_5H_5)_2]$ added to the test solutions as

an internal calibrant is 0.52 V. For the electrochemical studies at high scan rates a 50 μm platinum disc microelectrode was used as the working electrode with a silver and platinum wire used as the reference and auxiliary electrode, respectively. Fiber-optic difference IR spectroelectrochemical measurements were obtained as previously described.[63]

Calculations

All calculations were performed by using the Gaussian 03 package.[58] The B3LYP hybrid functional with the Stuttgart/Dresden SDD effective core potential basis set was used in all calculations.[64-67] The geometries of complexes for a given spin state were optimized and verified by performing Hessian calculations. The molecular orbital analyses were then conducted at those geometries.[58] The SOMO and LUMO three-dimensional isosurface plots were generated using the Avogadro program.[68]

[Co(tmhd)$_2$(phen)] 1. To a stirred purple solution of [Co(tmhd)$_2$] (0.0826 g, 0.2 mmol) in CH_2Cl_2 (15 cm^3), phen (0.0396 g, 0.2 mmol) was added. The orange solution was stirred for 1 hour at room temperature then filtered through celite. The solution was left to slowly evaporate at room temperature yields deep red needle crystals 0.0772 g (64%). Magnetic moment (μ_{eff}/μ_B, 297 K): 4.51. $C_{34}H_{46}N_2O_4Co$; calc. C 67.4, H 7.7, N 4.6; found C 67.5, H 7.4, N 5.6. Electrospray ionization (ESI) mass data: *m/z* 605 (100%, $[M]^+$), 422 (24%, $[M - tmhd]^+$).

[Co(tmhd)$_2$(2,2′-bpy)] 2. To a stirred purple solution of [Co(tmhd)$_2$] (0.0638 g, 0.15 mmol) in CH_2Cl_2 (5 cm^3), 2,2′-bpy (0.0240 g, 0.15 mmol) was added. The orange solution was stirred for 1 hour then filtered through celite. The solution was left to slowly evaporate at room temperature yields orange needle crystals 0.0451 g (53%). Magnetic moment (μ_{eff}/μ_B, 297 K): 4.53. $C_{32}H_{46}N_2O_4Co$; calc. C 66.1, H 8.0, N 4.8; found C 66.3, H 7.8, N 5.1. Electrospray ionization (ESI) mass data: *m/z* 581 (100%, $[M]^+$), 398 (20%, $[M - tmhd]^+$).

[Co(tmhd)$_2$(dmae)] 3. To a stirred purple solution of [Co(tmhd)$_2$] (0.0637 g, 0.15 mmol) in CH_2Cl_2 (10 cm^3), dmae (150 μL, 0.15 mmol) was added. The orange solution was stirred for 1 hour at room temperature then filtered through celite. The solution was left to slowly evaporate at room temperature yields deep red needle crystals 0.0313 g (54%). Magnetic moment (μ_{eff}/μ_B, 297 K): 4.53. $C_{26}H_{50}N_2O_4Co$; calc. C 60.8, H 9.8, N 5.4; found C 52.6, H 8.9, N 5.9. Electrospray ionization (ESI) mass data: *m/z* 513 (100%, $[M]^+$), 330 (8%, $[M - tmhd]^+$)..

[Co(dbm)$_2$(phen)] 4. To a stirred red-orange solution of [Co(dbm)$_2$] (0.0816 g, 0.15 mmol) in THF (20 cm^3) at 70 °C, phen (0.0301 g, 0.15 mmol) was added. The deep red solution was stirred for 1 hour at room temperature then filtered through celite. The solution was left to slowly evaporate at room temperature yields deep red needle crystals 0.0914 g (88%). Magnetic moment (μ_{eff}/μ_B, 297 K): 5.03.

$C_{42}H_{34}N_2O_4Co$; calc. C 73.1, H 5.0, N 4.1; found C 73.4, H 4.6, N 4.3. Electrospray ionization (ESI) mass data: *m/z* 689 (100%, $[M]^+$), 462 (18%, $[M - dbm]^+$).

$[Co(dbm)_2(2,2'\text{-bpy})]$ 5. To a stirred red-orange solution of $[Co(dbm)_2]$ (0.0811 g, 0.15 mmol) in THF (20 cm^3) at 70 °C, 2,2′-bpy (0.0234 g, 0.15 mmol) was added. The deep red solution was stirred for 1 hour at room temperature then the solution was left to slowly evaporate at room temperature yields deep red needle crystals 0.1014 g (100%). Magnetic moment (μ_{eff}/μ_B, 297 K): 4.41. $C_{40}H_{30}N_2O_4Co$; calc. C 72.6, H 4.6, N 4.2; found C 72.6, H 5.3, N 4.1. Electrospray ionization (ESI) mass data: *m/z* 661 $[M]^+$, 438 $[M - dbm]^+$. Electrospray ionization (ESI) mass data: *m/z* 661 (4%, $[M]^+$), 438 (100%, $[M - dbm]^+$).

$[Co(dbm)_2(dmae)]$ 6. To a stirred red-orange solution of $[Co(dbm)_2]$ (0.0811 g, 0.15 mmol) in THF (20 cm^3) at 70 °C, dmae (150 μL, 0.15 mmol) was added. The orange solution was stirred for 1 hour at room temperature then filtered through celite. The solution was left to slowly evaporate at room temperature yields deep red needle crystals 0.0646 g (73%). Magnetic moment (μ_{eff}/μ_B, 297 K): 4.98. $C_{34}H_{34}N_2O_4Co$; calc. C 68.8, H 5.7, N 4.7; found C 68.8, H 5.7, N 5.0 Electrospray ionization (ESI) mass data: *m/z* 593 (100%, $[M]^+$), 370 (68%, $[M - dbm]^+$)

$[Co(tmhd)_2(phen)][BF_4]$ 1^+. To a stirred purple solution of $[Co(tmhd)_2(H_2O)_2]$ (0.2303 g, 0.5 mmol) in CH_2Cl_2 (20 cm^3), phen (0.0992 g, 0.5 mmol) was added. The orange solution was stirred for 1 hour then $AgBF_4$ (0.110 g, 0.56 mmol) added. The brown-orange solution was stirred overnight. The dark green solution was filtered through celite then washed with CH_2Cl_2 (3 x 5 cm^3). The solvent was removed to dryness. The solid was purified using CH_2Cl_2-diethyl ether to give dark red block crystals yield 0.2120 g (61%). $C_{34}H_{46}BCoF_4N_2O_4$; calc. C 59.0, H 6.7, N 4.0; found C 58.7, H 6.9, N 4.3. Electrospray ionization (ESI) mass data: *m/z* 605 (100%, $[M - BF_4]^+$), 422 (35%, $[M - BF_4 - tmhd]^+$).

$[Co(tmhd)_2(2,2'\text{-bpy})][BF_4]$ 2^+. To a stirred purple solution of $[Co(tmhd)_2(H_2O)_2]$ (0.2330 g, 0.5 mmol) in CH_2Cl_2 (20 cm^3), 2,2′-bpy (0.0785 g, 0.5 mmol) was added. The orange solution was stirred for 1 hour then $AgBF_4$ (0.110 g, 0.56 mmol) added. The brown-orange solution was stirred overnight. The dark green solution was filtered through celite then washed with CH_2Cl_2 (3 x 5 cm^3). The solvent was removed to dryness. The solid was purified using CH_2Cl_2-diethyl ether to give maroon microcrystals yield 0.2138 g (64%). $C_{32}H_{46}BCoF_4N_2O_4$; calc. C 57.5, H 6.9, N 4.2; found C 57.5, H 6.9, N 4.6. Electrospray ionization (ESI) mass data: *m/z* 581 (100%, $[M - BF_4]^+$), 398 (42%, $[M - BF_4 - tmhd]^+$).

$[Co(tmhd)_2(dmae)][BF_4]$ 3^+. To a stirred purple solution of $[Co(tmhd)_2(H_2O)_2]$ (0.2298 g, 0.5 mmol) in CH_2Cl_2 (20 cm^3), dmae (54.4 μL, 0.5 mmol) was added. The orange solution was stirred for 1 hour then $AgBF_4$ (0.110 g, 0.56 mmol) added. The dark green solution was stirred overnight. The deep purple solution was filtered through celite then washed with CH_2Cl_2 (3 x 5 cm^3). The solvent was removed to dryness. The solid was purified using CH_2Cl_2-diethyl ether to give pastel purple microcrystals yield

0.1841 g (61%). $C_{26}H_{50}BCoF_4N_2O_4$; calc. C 52.0, H 8.4, N 4.7; found C 52.7, H 8.6, N 5.2. Electrospray ionization (ESI) mass data: *m/z* 513 (100%, $[M - BF_4]^+$), 330 (94%, $[M - BF_4 - tmhd]^+$).

$[Co(dbm)_2(phen)][BF_4]$ 4^+. To a stirred orange suspension of $[Co(dbm)_2(H_2O)_2]$ (0.1678 g, 0.3 mmol) in CH_2Cl_2 (20 cm^3), phen (0.0620 g, 0.3 mmol) was added. The orange solution was stirred for 1 hour then $AgBF_4$ (0.0700 g, 0.36 mmol) added. The olive green solution was stirred overnight. The dark green solution was filtered through celite then washed with CH_2Cl_2 (3 x 5 cm^3). The solvent was removed to dryness. The solid was purified using CH_2Cl_2-*n*-hexane to give olive green microcrystals yield 0.1295 g (56%). $C_{42}H_{34}BCoF_4N_2O_4$; calc. C 65.0, H 4.4, N 3.6; found C 66.5, H 4.2, N 3.9. Electrospray ionization (ESI) mass data: *m/z* 689 (84%, $[M - BF_4]^+$), 462 (100%, $[M - BF_4 - dbm]^+$).

$[Co(dbm)_2(2,2'\text{-bpy})][BF_4]$ 5^+. To a stirred orange suspension of $[Co(dbm)_2(H_2O)_2]$ (0.1586 g, 0.3 mmol) in CH_2Cl_2 (20 cm^3), 2,2′-bpy (0.0470 g, 0.3 mmol) was added. The orange solution was stirred for 1 hour then $AgBF_4$ (0.0646 g, 0.33 mmol) added. The olive green solution was stirred overnight. The dark green solution was filtered through celite then washed with CH_2Cl_2 (3 x 5 cm^3). The solvent was removed to dryness. The solid was purified using CH_2Cl_2-*n*-hexane to give green brown microcrystals yield 0.1097 g (51%). $C_{40}H_{30}BCoF_4N_2O_4$; calc. C 64.2, H 4.0, N 3.7; found C 65.2, H 4.3, N 3.9. Electrospray ionization (ESI) mass data: *m/z* 661 (54%, $[M - BF_4]^+$), 438 (100%, $[M - BF_4 - dbm]^+$).

$[Co(dbm)_2(dmae)][BF_4]$ 6^+. To a stirred orange suspension of $[Co(dbm)_2(H_2O)_2]$ (0.1718 g, 0.3 mmol) in CH_2Cl_2 (20 cm^3), dmae (34.7 μL, 0.3 mmol) was added. The orange solution was stirred for 1 hour then $AgBF_4$ (0.0710 g, 0.36 mmol) added. The olive green solution was stirred overnight. The dark green solution was filtered through celite then washed with CH_2Cl_2 (3 x 5 cm^3). The solvent was removed to dryness. The solid was purified using CH_2Cl_2-*n*-hexane to give olive green microcrystals yield 0.1072 g (49%). $C_{34}H_{34}BCoF_4N_2O_4$; calc. C 60.0, H 5.0, N 4.1; found C 62.7, H 5.3, N 3.7. Electrospray ionization (ESI) mass data: *m/z* 593 (84%, $[M - BF_4]^+$), 370 (100%, $[M - BF_4 - dbm]^+$).

ACKNOWLEDGMENTS We thank the Walailak University Research Fund (grant number 5/2549) and the Thailand Research Fund (RSA5080007 and RSA5180010) for partial financial support. Computational resources: National Nanotechnology Center (NANOTEC) Thailand.

FIGURE CAPTIONS

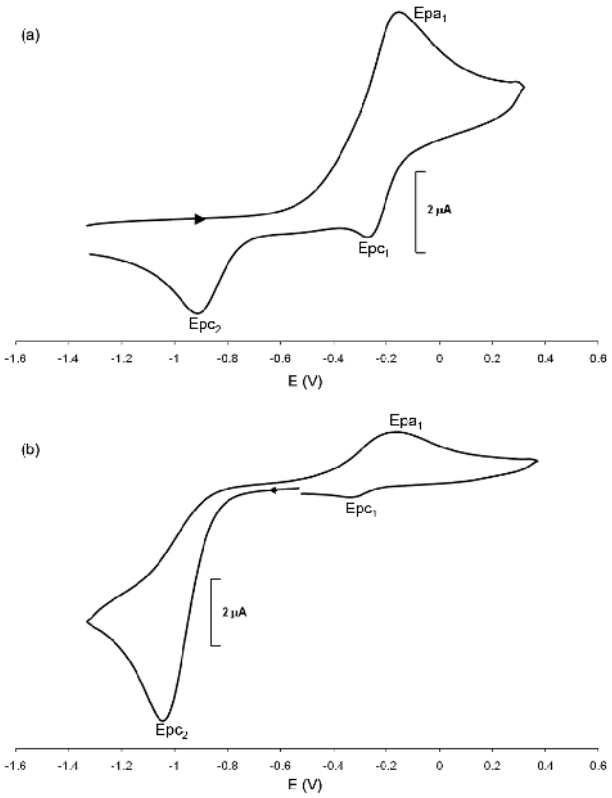

Figure 1. Cyclic voltammograms of (a) [Co(tmhd)$_2$(phen)] **1** (b) [Co(tmhd)$_2$(phen)][BF$_4$] **1**$^+$[BF$_4$].

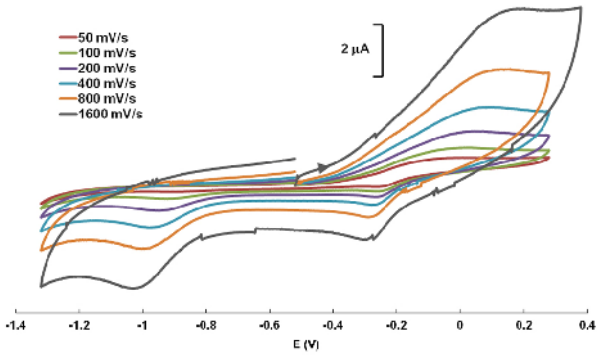

Figure 2. Cyclic voltammograms of [Co(tmhd)$_2$(phen)] at scan rates of 50 to 1600 mV/s.

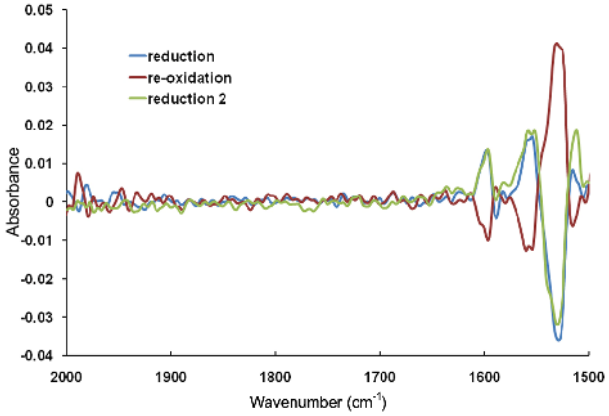

Figure 3. IR spectroelectrochemical difference spectra of $[Co(dbm)_2(phen)][BF_4]$ $\mathbf{4}^{+}[BF_4]$.

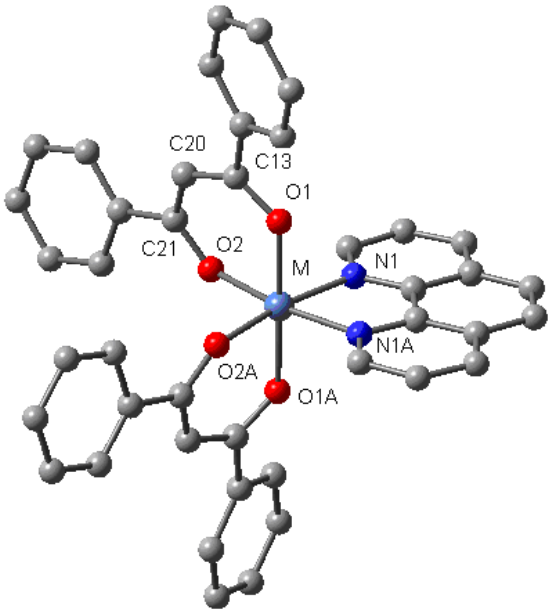

Figure 4. Numbering scheme for $[Co(dbm)_2(phen)]$ complex as used for structural comparison with the X-ray structures.

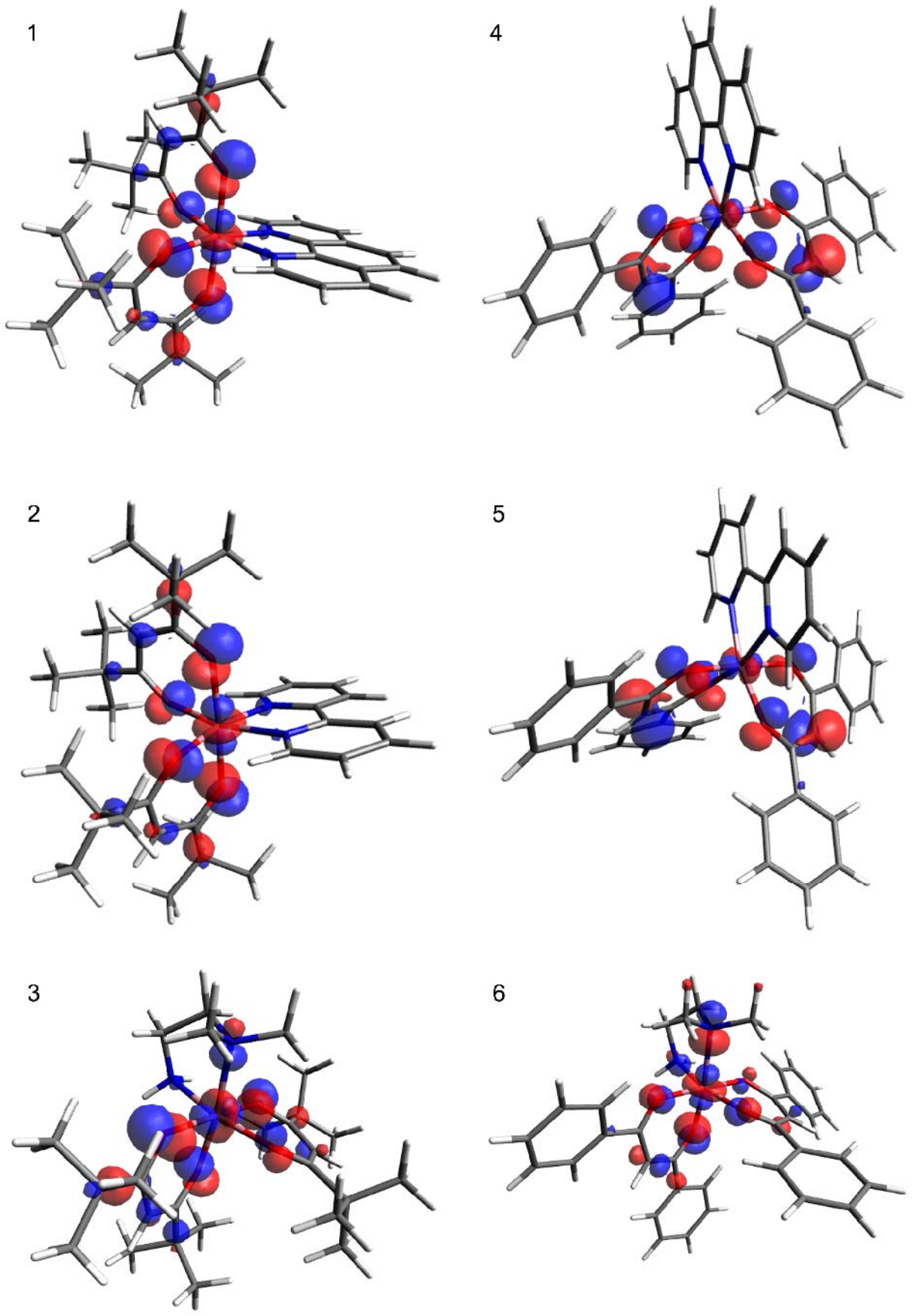

Figure 5. The SOMO orbital of complexes **1-6**

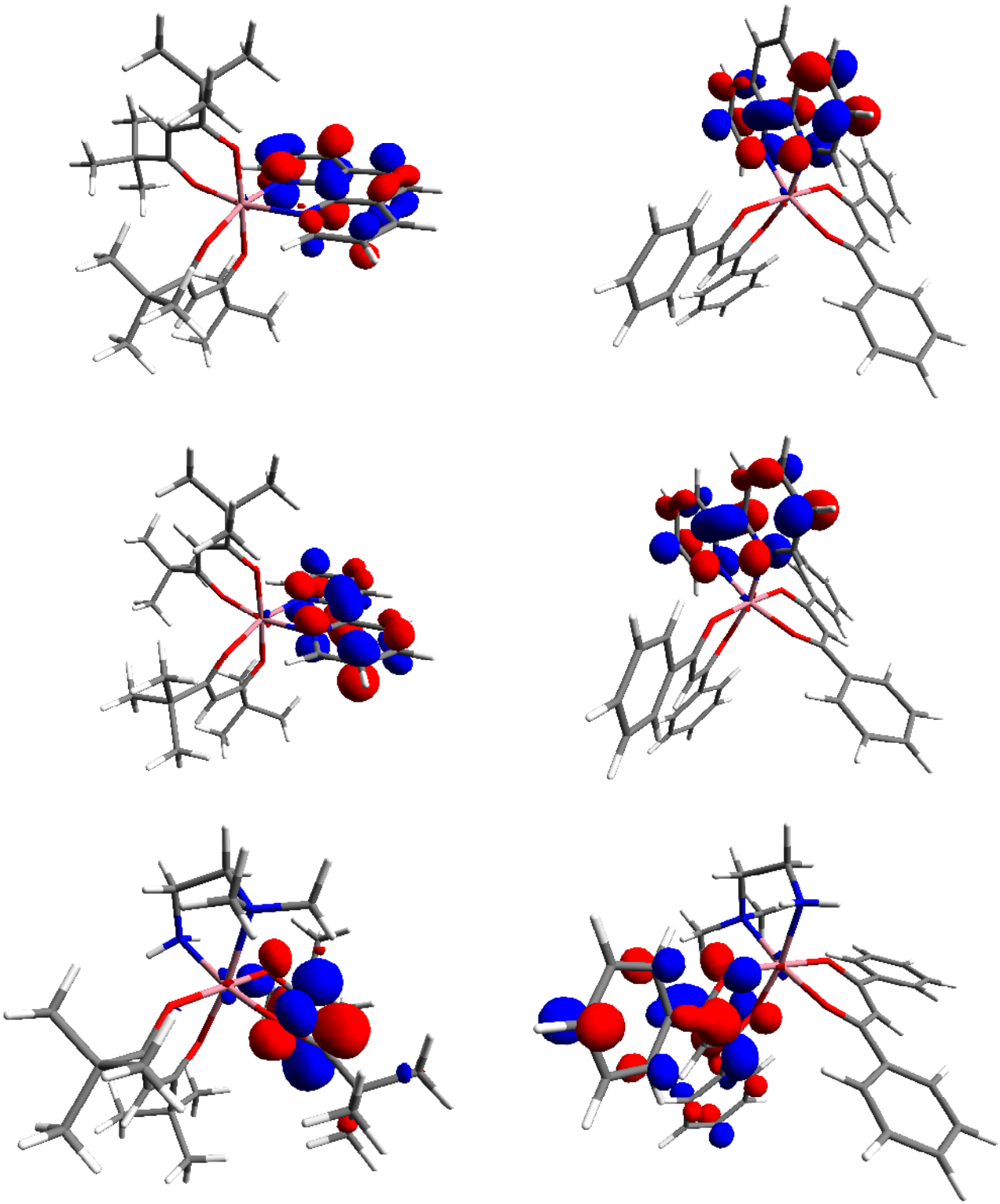

Figure 6. The LUMO orbital of complexes **1-6**

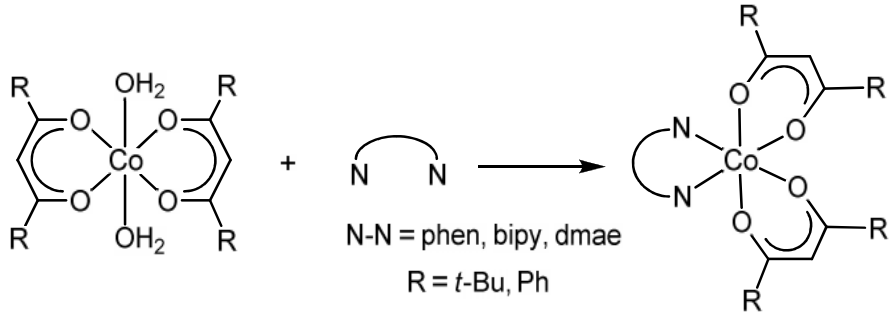

Scheme 1. Synthesis of [Co(β-diketonate)$_2$(N-N)].

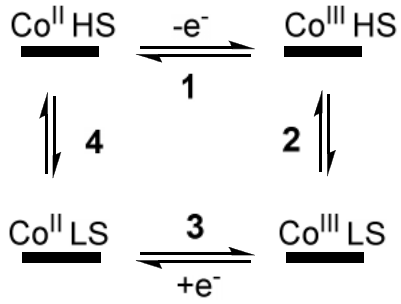

Scheme 2. Square scheme of the redox coupled-spin crossover process showing individual spin crossover and electron transfer processes.

Table 1. IR and UV-Vis spectroscopic data for [Co(β-diketonate)$_2$(N-N)] complexes.

Complex	% Yield	Color	IR		λ/nm(log ε/mol^{-1} dm^3 cm^{-1})
			$\nu_{C=O}$	ν_{N-H}	
[Co(tmhd)$_2$(phen)] **1**	64	Deep red		-	268 (5.00), 289 (4.77, sh), 399 (3.03, sh), 438 (3.09), 532 (2.47, sh)
[Co(tmhd)$_2$(2,2′-bpy)] **2**	53	Orange	1561	-	288 (4.85), 430 (3.02), 541 (3.37)
[Co(tmhd)$_2$(dmae)] **3**	54	Deep red	1583	3365	268 (4.49), 345 (3.72, sh), 554 (2.10)
[Co(dbm)$_2$(phen)] **4**	88	Red	1595	-	268 (5.02), 287 (4.64, sh), 349 (4.81), 368 (4.55, sh), 413 (3.40)
[Co(dbm)$_2$(2,2′-bpy)] **5**	100	Red	1596	-	291 (4.62), 351 (4.75), 370 (4.54, sh), 415 (3.43), 549 (2.09, sh)
[Co(dbm)$_2$(dmae)] **6**	73	Red	1594	-	345 (4.34), 382 (3.85), 548 (1.99)
[Co(tmhd)$_2$(phen)]$^+$ **1**$^+$	61	Dark red	1543	-	268 (4.48), 298 (4.17, sh), 344(3.63, sh), 576 (2.18)
[Co(tmhd)$_2$(2,2′-bpy)]$^+$ **2**$^+$	64	Maroon	1545	-	299 (4.67), 309 (4.65), 341 (4.12), 569 (2.22)
[Co(tmhd)$_2$(dmae)]$^+$ **3**$^+$	61	Pastel purple	1560	3310, 3264	300 (4.32, sh), 337 (4.00), 574 (2.28)
[Co(dbm)$_2$(phen)]$^+$ **4**$^+$	56	Olive green	1524	-	273 (4.54), 292 (4.50, sh), 350 (3.91), 376 (3.92), 578 (2.37)
[Co(dbm)$_2$(2,2′-bpy)]$^+$ **5**$^+$	51	Brown green	1524	-	262 (4.96, sh), 292 (5.15), 382 (4.56), 413 (3.43), 422 (3.40), 574 (2.40)
[Co(dbm)$_2$(dmae)]$^+$ **6**$^+$	49	Olive green	1525	3320, 3264	284 (5.07), 384 (4.50), 415 (3.42), 427 (3.40), 578 (2.33)

Table 2. Cyclic voltammetric data of [Co(β-diketonate)$_2$(N-N)].

Complex	Peak potential (V)		
	Epa_1	Epc_1	Epc_2
[Co(tmhd)$_2$(phen)] **1**	-0.15	-0.27	-1.18
[Co(tmhd)$_2$(2,2′-bpy)] **2**	-0.11	-	-1.08
[Co(tmhd)$_2$(dmae)] **3**	-0.13	-	-1.32
[Co(dbm)$_2$(phen)] **4**	0.03	-0.37	-0.98
[Co(dbm)$_2$(2,2′-bpy)] **5**	-0.07	-0.38	-0.61
[Co(dbm)$_2$(dmae)] **6**	0.06	-0.43	-1.21
[Co(tmhd)$_2$(phen)][BF_4] $\mathbf{1}^+$	-0.17	-0.34	-1.38
[Co(tmhd)$_2$(2,2′-bpy)][BF_4] $\mathbf{2}^+$	-0.24	-0.38	-1.41
[Co(tmhd)$_2$(dmae)][BF_4] $\mathbf{3}^+$	-0.08	-0.31	-1.53
[Co(dbm)$_2$(phen)][BF_4] $\mathbf{4}^+$	0.00	-0.22	-0.86
[Co(dbm)$_2$(2,2′-bpy)][BF_4] $\mathbf{5}^+$	-0.06	-	-0.73
[Co(dbm)$_2$(dmae)][BF_4] $\mathbf{6}^+$	-0.17	-	-0.72

All measurements were performed at 298 K, in dried and degassed CH_2Cl_2 0.1 M [NBu^n_4][PF_6] solution; scan rate 100 mVs^{-1}; calibrated with [$FeCp_2$], and reported relative to the $[FeCp_2]^{0/+}$ couple.

Table 3. ^{1}H NMR spectroscopic data of [Co(β-diketonate)$_2$(N-N)][BF_4] complexes.

Complex	δ (ppm)
[Co(tmhd)$_2$(phen)][BF_4] **1**$^+$	8.98 (2H, dd, J_{HH} 0.6 Hz, 8.1 Hz, C*H*^{Phen}), 8.38 (2H, d, J_{HH} 5.4 Hz, C*H*^{Phen}), 8.34 (2H, s, C*H*^{Phen}), 8.15 (2H, dd, J_{HH} 8.1 Hz, 5.4 Hz, C*H*^{Phen}), 5.91 (2H, s, C*H*^{central}), 1.31 (18H, s, *t*-Bu), 0.80 (18H, s, *t*-Bu)
[Co(tmhd)$_2$(2,2′-bpy)][BF_4] **2**$^+$	8.90 (2H, d, J_{HH} 7.8 Hz, *H*$^{6,\ bpy}$), 8.42 (2H, t, J_{HH} 7.8 Hz, 6.3 Hz, *H*$^{5,\ bpy}$), 8.12 (2H, d, J_{HH} 5.1 Hz, *H*$^{3,\ bpy}$), 7.70 (2H, t, J_{HH} 6.3 Hz, 5.1 Hz, *H*$^{4,\ bpy}$), 5.86 (2H, s, C*H*^{central}), 1.32 (18H, s, *t*-Bu), 0.87 (18H, s, *t*-Bu)
[Co(tmhd)$_2$(dmae)][BF_4] **3**$^+$	5.87 (1H, s, C*H*^{central}), 5.80 (1H, s, C*H*^{central}), 4.00 (2H, s, N-C*H$_2$*), 2.80 (2H, s, N-C*H$_2$*), 2.39 (3H, s, N-C*H$_3$*), 1.80 (3H, s, N-C*H$_3$*), 1.21 (18H, s, *t*-Bu), 1.12 (9H, s, *t*-Bu), 1.05 (9H, s, *t*-Bu)
[Co(dbm)$_2$(phen)][BF_4] **4**$^+$	9.01 (2H, dd, J_{HH} 8.1 Hz, 0.9 Hz, C*H*^{Phen}), 8.70 (2H, d, J_{HH} 5.1 Hz, C*H*^{Phen}), 8.40 (2H, s, C*H*^{Phen}), 8.12 (2H, dd, J_{HH} 8.1 Hz, 5.1 Hz, C*H*^{Phen}), 8.04 (4H, m, *H*^{Ph}), 7.60-7.55 (6H, m, *H*^{Ph}), 7.50-7.40 (6H, m, *H*^{Ph}), 7.32-7.28 (4H, m, *H*^{Ph}), 7.01 (2H, s, C*H*^{central})
[Co(dbm)$_2$(2,2′-bpy)][BF_4] **5**$^+$	9.03 (2H, d, J_{HH} 7.50 Hz, *H*$^{6,\ bpy}$), 8.47 (4H, m, *H*$^{6,\ bpy}$, *H*$^{3,\ bpy}$), 7.98 (4H, d, J_{HH} 7.20 Hz, *H*^{Ph}), 7.70 (2H, t, J_{HH} 6.90 Hz, *H*$^{4,\ bpy}$), 7.64 (4H, d, J_{HH} 7.20 Hz, *H*^{Ph}), 7.55-7.34 (12H, m, *H*^{Ph}), 6.97 (2H, s, C*H*^{central})
[Co(dbm)$_2$(dmae)][BF_4] **6**$^+$	8.10 (2H, d, J_{HH} 6.90 Hz, *H*^{Ph}), 7.97 (3H, m, *H*^{Ph}), 7.91 (2H, d, J_{HH} 7.2 Hz, *H*^{Ph}), 7.71 (2H, d, J_{HH} 7.50 Hz, *H*^{Ph}), 7.59-7.50 (9H, m, *H*^{Ph}), 7.42-7.37 (4H, m, *H*^{Ph}), 6.97 (1H, s, C*H*^{central}), 6.81 (1H, s, C*H*^{central}), 4.70 (1H, broad, s, N-C*H$_2$*), 4.50 (1H, broad, s, N-C*H$_2$*), 3.2 (1H, broad, s, N-C*H$_2$*), 2.8 (1H, broad, s, N-C*H$_2$*), 2.56 (3H, s, N-C*H$_3$*), 2.01 (3H, s, N-C*H$_3$*)

Table 4. IR spectroelectrochemical difference data of [Co(β-diketonate)$_2$(N-N)] complexes.

Complex	Bands of species produced (cm^{-1})	Bands of starting material consumed (cm^{-1})
[Co(tmhd)$_2$(phen)] **1** [a]	1552, 1543, 1523	1587, 1572, 1533, 1516, 1505
[Co(tmhd)$_2$(2,2′-bpy)] **2** [a]	1545, 1527	1588, 1581, 1570, 1518, 1504
[Co(tmhd)$_2$(dmae)] **3** [a]	1557, 1547, 1533	1592, 1582, 1570
[Co(dbm)$_2$(phen)] **4** [a]	1587, 1528	1596, 1564, 1554, 1514
[Co(dbm)$_2$(2,2′-bpy)] **5** [a]	1530	1597, 1563, 1549
[Co(dbm)$_2$(dmae)] **6** [a]	1526	1563, 1553
[Co(tmhd)$_2$(phen)]$^+$ **1**$^+$ [b]	1589, 1573, 1506	1558, 1548, 1525
[Co(tmhd)$_2$(2,2′-bpy)]$^+$ **2**$^+$ [b]	1587, 1572, 1506	1552 (sh), 1544, 1531, 1496
[Co(tmhd)$_2$(dmae)]$^+$ **3**$^+$ [b]	1596, 1581, 1569	1546, 1534
[Co(dbm)$_2$(phen)]$^+$ **4**$^+$ [b]	1596, 1557, 1552, 1512	1538 (sh), 1529
[Co(dbm)$_2$(2,2′-bpy)]$^+$ **5**$^+$ [b]	1597, 1579, 1554, 1513	1530, 1588
[Co(dbm)$_2$(dmae)]$^+$ **6**$^+$ [b]	1596, 1557, 1516	1588, 1540, 1528

[a] Oxidized at ca Epa_1. [b] Reduced at Epc_2

Table 5. Selected computed and X-ray crystallographically determined bond lengths (Å) and bond angles (^{o}) for [Co(dbm)$_2$(phen)]. See Figure 4 for the numbering scheme.

[Co(dbm)$_2$(phen)]	X-ray[1]	Doublet	diff.[2]	Quartet	diff.[2]
Co-O1	2.07	2.15	0.08	2.0627	0.01
Co-O2	2.07	1.94	0.13	2.0544	0.01
Co-N1	2.15	1.96	0.19	2.1493	0.00
C7-O1	1.28	1.29	0.01	1.3022	0.02
C20-O2	1.27	1.31	0.04	1.3052	0.03
C7-C21	1.41	1.43	0.02	1.4019	0.00
C20-C21	1.41	1.41	0.00	1.4163	0.01
O1-Co-O2	86.29	88.63	2.34	85.73	0.56
O2-Co-O2A	102.54	91.92	10.62	98.69	3.85
O1-Co-O2A	83.67	89.01	5.34	91.96	8.29
O1-Co-N1	101.53	92.85	8.68	96.11	5.42
O1-Co-N1A	91.10	89.67	1.43	86.68	4.42
O2-Co-N1	90.49	92.24	1.75	92.43	1.94
O1-Co-O1A	163.92	176.63	12.71	176.42	12.50
N1-Co-N1A	76.87	83.64	6.77	77.58	0.71

[1]From ref. 59.
[2]Difference between X-ray crystallographic and optimized structure.

Table 6. The high-spin and low-spin complex energy difference, E(HS)-E(LS), at B3LYP/SDD level for [Co(β-diketonate)$_2$(N-N)] complexes. For **1**$^+$**-6**$^+$**,** the pentet and triplet (in parenthesis) HS states were considered. The E(LUMO)-E(SOMO) gap was estimated from the alpha spin orbital energy of the most stable spin state.

Complex	E(HS)-E(LS)/(kcal.mol^{-1})	E(LUMO)-E(SOMO)/eV
[Co(tmhd)$_2$(phen)] **1**	-15.63	2.91
[Co(tmhd)$_2$(2,2′-bpy)] **2**	-14.55	2.91
[Co(tmhd)$_2$(dmae)] **3**	-12.67	4.54
[Co(dbm)$_2$(phen)] **4**	-13.84	3.13
[Co(dbm)$_2$(2,2′-bpy)] **5**	-12.80	2.86
[Co(dbm)$_2$(dmae)] **6**	-13.26	3.75
[Co(tmhd)$_2$(phen)]$^+$ **1**$^+$	16.12 (16.38)	3.48
[Co(tmhd)$_2$(2,2′-bpy)]$^+$ **2**$^+$	17.15 (17.19)	3.40
[Co(tmhd)$_2$(dmae)]$^+$ **3**$^+$	17.41 (17.60)	4.27
[Co(dbm)$_2$(phen)]$^+$ **4**$^+$	16.93 (17.31)	3.29
[Co(dbm)$_2$(2,2′-bpy)]$^+$ **5**$^+$	18.01 (18.16)	3.24
[Co(dbm)$_2$(dmae)]$^+$ **6**$^+$	17.93 (16.61)	3.70

REFERENCES

1. Létard, J.-F.; Guionneau, P.; Goux-Capes, L. *Top. Curr. Chem*. **2004**, *235*, 221.
2. Kahn, O. Martinez, C. J. *Science* **1998**, *279*, 44.
3. Fabbrizzi, L.; Licchelli, M.; Pallavicini, P. *Acc. Chem. Rev*. **1999**, *32*, 846.
4. Venturi, M.; Credi, A.; Balzani, V. *Coord. Chem. Rev*. **1999**,
5. H. A. Goodwin, *Coord. Chem. Rev.* **1976**, **18**, 293.
6. (a) Real, J. A.; Gaspar, A. B.; Niel, V.; Muñoz, M. C. *Coord. Chem. Rev.* **2003**, *236*, 121. (b) Garcia, Y.; Niel, V.; Muñoz, M. C. and Real, J. A. *Top. Curr. Chem.* **2004**, *233*, 229.
7. Murray, K. S.; Kepert, C. J. *Top. Curr. Chem.* **2004**, *233*, 195.
8. Gaspar, A. B.; Ksenofontov, V.; Real, J. A.; Gütlich, P. *Chem. Phys. Lett.* **2003**, *373*, 385.
9. (a) Spiering, H.; Kohlhaas, T.; Romstedt, H.; Hauser, A.; Bruns-Yilmaz, C.; Gütlich, P. *Coord. Chem. Rev.* **1999**, *190–192*, 629. (b) Gütlich, P.; Hauser, A.; Spiering, H. *Angew. Chem., Int. Ed. Engl.* **1994**, *33*, 2024.
10. (a) Real, J. A. in *Transition Metals in Supramolecular Chemistry*, ed. Sauvage, J. P. John Wiley and Sons, Ltd., Chichester, **1999**, p. 53. (b) Real, J. A.; Gaspar, A. B.; Muñoz, M. C.; Gütlich, P.; Ksenofontov, V.; Spiering, H. *Top. Curr. Chem.* **2004**, *233*, 167.
11. Haasnoot, J. G. *Coord. Chem. Rev.* **2000**, *200*, 131.
12. Breuning, E.; Ruben, M.; Lehn, J. M.; Renz, F.; Garcia, Y.; Ksenofontov, V.; Gütlich, P.; Wegelius, E.; Rissanen, K. *Angew. Chem., Int. Ed.* **2000**, *39*, 2504.
13. Real, J. A.; Andres, E.; Muñoz, M. C.; Julve, M.; Granier, T.; Bousseksou, A.; Varret, F. *Science* **1995**, *268*, 265.
14. Halder, G. J.; Kepert, C. J.; Moubaraki, B.; Murray, K. S.; Cashion, J. D. *Science* **2002**, *298*, 1762.
15. Madeja, K.; König, E. *J. Inorg. Nucl. Chem*. **1963**, *25*, 377.
16. Sieber, R.; Decurtins, S.; Stoeckli, H.; Evans, C.; Wilson, D.; Yufit, J. A. K.; Howard, S. C.; Capelli, A.; Hauser, A. *Chem. Eur. J*. **2000**, *6*, 361.

17. (a) Zerara, M.; Hauser, A. *Chem. Phys. Chem*. **2004**, *5*, 395. (b) Hauser A.; Amstutz, N.; Delahaye, S.; Schenker, S.; Sadki, A.; Sieber, R.; Zerara, M. *Struct. Bond*. **2004**, *106*, 81.
18. (a) Hogg, R.; Wilkins, R. G. *J. Chem. Soc*. **1962**, 341. (b) Judge, J. S.; Baker, W. A. *Inorg. Chim. Acta* **1967**, *1*, 68.
19. Figgis, B. N.; Kucharski, E. S.; White, A.H. *Aust. J. Chem*. **1983**, 36, 1537.
20. Scheidt, W. R.; Reed, C. A. *Chem*. *Rev*. **1981**, *81*, 543.
21. Bertani, I.; Gray, H. B.; Lippard, S. J.; Valentine, J. S. *Bioinorganic Chemistry*, University Science Books, Sausalito, CA, **1994**.
22. Lippard, S. J.; Berg, J. M. *Principles of Bioinorganic Chemistry*, University Science Books, Mill Balley, CA, **1995**.
23. Kaim, W.; Schwederski, B. *Bioinorganic Chemistry: Inorganic Elements in the Chemistry of Life*, Wiley, New York, **1995**.
24. Sligar, S. C. *Biochemistry* **1976**, *15*, 5399.
25. Mueller, E. J.; Lioda, P. J.; Sligar, S. C. in *Cytochrome P450: Structure, Mechanism and Biochemistry*, ed. Ortiz de Montellano, P.R. 2nd ed., Plenum Press, New York, **1995**, Chap. 3.
26. Rees, D. C.; Chan, M. K.; Kim, J. *Adv. Inorg. Chem*. **1993**, *40*, 89.
27. Burgess, B. K.; Lowe, D. J. *Chem. Rev*. **1996**, *96*, 2983.
28. Lopes, H.; Pettigrew, G. W.; Moura, I.; Moura, J. J. G. *J. Biol. Inorg. Chem*. **1998**, *3*, 632.
29. Hendry, P.; Ludi, A. *Adv. Inorg. Chem*. **1990**, *35*, 117.
30. Stynes, H.C.; Ibers, J.A. *Inorg. Chem*. **1971**, *10*, 2304.
31. Buhks, E.; Bixon, M.; Jortner, J.; Navon, G. *Inorg. Chem*. **1979**, *18*, 2014.
32. Geselowitz, D.A., Taube, H. *Adv. Inorg. Bioinorg. Mech*. **1982**, *1*, 391.
33. Larsson, S.; Ståhl, K.; Zerner, M.C. *Inorg. Chem*. **1986**, *25*, 3033.
34. Geselowitz, D.A. *Inorg. Chim. Acta* **1988**, *154*, 225.
35. Newton, M.D. *J. Phys. Chem.* **1991**, *95*, 30.
36. Shalders, R.D.; Swaddle, T.W. *Inorg. Chem*. **1995**, *34*, 4815.

37. Swaddle, T.W. *Can. J. Chem*. **1996**, *74*, 631.

38. Turner, J. W.; Schultz, F. A. *Inorg. Chem*. **1999**, *38*, 358.

39. Turner, J. W.; Schultz, F. A. *J. Phys. Chem. B* **2002**, *106*, 2009.

40. Lord, R. L.; Schultz, F. A., Baik, M.-H. *J. Am. Chem. Soc*. **2009**, *131*, 6189.

41. Nakamoto, K. in *Infrared and Raman Spectra of Inorganic and Coordination Compounds: Part B*, 6th ed., Wiley, New York, **2009**, pp. 96-104.

42. Harding, P.; Harding, D. J.; Phonsri, W.; Saithong, S.; Phetmung, H. *Inorg. Chim. Acta* **2009**, *362*, 78.

43. Cotton, F.A.; Wilkinson, G.; Murillo, C.A.; Bochmann, M. in *Advanced Inorganic Chemistry*, 6th ed.; John Wiley & Sons, New York, **1999**, pp. 817-822.

44. Bandoli, G.; Barreca, D.; Gasparotto, A.; Maccato, C.; Seraglia, R.; Tondello, E.; Devi, A.; Fischer, R. A.; Winter, M. *Inorg. Chem.* **2009**, *48*, 82.

45. Nagashima, N.; Kudoh, S.; Nakata, M. *Chem. Phys. Lett.* **2003**, *374*, 59.

46. Sankhla, D. S.; Mathur, R. C.; Misra, S. N. *J. Inorg. Nuc. Chem.* **1980**, *42*, 489.

47. Chassot, P.; Emmenegger, F. *Inorg. Chem.* **1996**, *35*, 5931.

48. Archer, R. D.; Cotsoradis, B. P. *Inorg. Chem.* **1965**, *4,* 1584.

49. York, R. J.; Bonds, W.D. Jr.; Cotsoradis, B. P.; Archer, R. A. *Inorg. Chem.* **1969**, *8*, 789.

50. Izumi, F.; Kurosawa, R.; Kawamoto, H.; Akaiwa, H. *Bull. Chem. Soc. Jpn.* **1975**, *48*, 3188.

51. Turner, J. W.; Schultz, F. A. *Coord. Chem. Rev.* **2001**, *219-221*, 81.

52. For examples of other Co complexes exhibiting RCSCO see (a) Buhks, E.; Dixon, M.; Jortner, J.; Navon, G. *Inorg. Chem.* **1979**, *18*, 2014. (b) Endicott, J. F.; Brubaker, G. R.; Ramasami, T.; Kumar, K.; Dwarakanath, K.; Cassel, J.; Johnson, D. *Inorg. Chem.* **1983**, *22*, 3754. (c) Hammershøi, A.; Geselowitz, D.; Taube, H. *Inorg. Chem.* **1984**, *32*, 979. (d) Bernhardt, P. V.; Jones, L. A.; Sharpe, P. C. *Inorg. Chem.* **1997**, *36*, 2420.

53. Johansson, F. B.; Bond, A. D.; Nielson, U. G.; Moubaraki, B.; Murray, K. S.; Berry, K. J.; Larrabee, J. A.; McKenzie, C. J. *Inorg. Chem*. **2008,** *47*, 5079.

54. De Alwis, D. C. L.; Schultz, F. A. *Inorg. Chem.* **2003**, *42*, 3616.

55. Wieghardt, K.; Schmidt, W.; Herrmann, W.; Kueppers, H. J. *Inorg. Chem*. **1983**, *22*, 2953.

56. Kueppers, H. J.; Neves, A.; Pomp, C.; Ventur, D.; Wieghardt, K.; Nuber, B.; Weiss, J. *Inorg. Chem*. **1986**, *25*, 2400.

57. Richards, T. C.; Geiger, W.E. *J. Am. Chem. Soc.* **1994**, *116*, 2028.

58. Gaussian 03, Revision D.01, Frisch, M. J.; Trucks, G. W.; Schlegel, H. B.; Scuseria, G. E.; Robb, M. A.; Cheeseman, J. R.; Montgomery, Jr., J. A.; Vreven, T.; Kudin, K. N.; Burant, J. C.; Millam, J. M.; Iyengar, S. S.; Tomasi, J.; Barone, V.; Mennucci, B.; Cossi, M.; Scalmani, G.; Rega, N.; Petersson, G. A.; Nakatsuji, H.; Hada, M.; Ehara, M.; Toyota, K.; Fukuda, R.; Hasegawa, J.; Ishida, M.; Nakajima, T.; Honda, Y.; Kitao, O.; Nakai, H.; Klene, M.; Li, X.; Knox, J. E.; Hratchian, H. P.; Cross, J. B.; Bakken, V.; Adamo, C.; Jaramillo, J.; Gomperts, R.; Stratmann, R. E.; Yazyev, O.; Austin, A. J.; Cammi, R.; Pomelli, C.; Ochterski, J. W.; Ayala, P. Y.; Morokuma, K.; Voth, G. A.; Salvador, P.; Dannenberg, J. J.; Zakrzewski, V. G.; Dapprich, S.; Daniels, A. D.; Strain, M. C.; Farkas, O.; Malick, D. K.; Rabuck, A. D.; Raghavachari, K.; Foresman, J. B.; Ortiz, J. V.; Cui, Q.; Baboul, A. G.; Clifford, S.; Cioslowski, J.; Stefanov, B. B.; Liu, G.; Liashenko, A.; Piskorz, P.; Komaromi, I.; Martin, R. L.; Fox, D. J.; Keith, T.; Al-Laham, M. A.; Peng, C. Y.; Nanayakkara, A.; Challacombe, M.; Gill, P. M. W.; Johnson, B.; Chen, W.; Wong, M. W.; Gonzalez, C.; and Pople, J. A.; Gaussian, Inc., Wallingford CT, 2004.

59. Meštrović, E; Kaitner, B. *J. Chem. Crystallogr*. **2006**, *36*, 599.

60. Barreca, D.; Massignan, C.; Daolio, S.; Fabrizio, M.; Piccirillo, C.; Armelao, L.; Tondello, E. *Chem. Mater.* **2001**, *13*, 588.

61. Barrios, L. A.; Ribas, J.; Aromí, G.; Ribas-Ariño, J.; Gamez, P.; Roubeau, O.; Teat, S. J. *Inorg. Chem.* **2007**, *46*, 7154.

62. Evans, D. F. *J. Chem. Soc.* **1959**, 2003–2005.

63. Shaw, M. J., Henson, R. L., Houk, S. E., Westhoff, J. W., Richter-Addo, G. B., Jones, M. W. *J. Electroanal. Chem.* **2002**, *534*, 47

64. Becke, A. D. *J. Chem. Phys*. **1993**, *98*, 1372.

65. Stephens, P. J.; Devlin, F. J.; Frisch, M. J.; Chabalowski, C. F. *J. Phys. Chem.* **1994**, *98*, 11623.

66. Dunning Jr., T. H.; Hay, P. J. in *Modern Theoretical Chemistry*, ed. H. F. Schaefer III, Vol. 3 Plenum, New York, **1976**, pp. 1-28.

67. Dolg, M.; Wedig, U.; Stoll, H.; Preuss, H. *J. Chem. Phys.* 86, **1987**, 866.

68. http://avogadro.openmolecules.net/ accessed 12/22/2009.

Appendix Five

Oral presentation at the Pure and Applied Chemistry International Conference (PACCON2011)

Electronic Communication Between Two Metal β-Diketonate Complexes Bridged by Diimine Linkers

Phimphaka Harding

Molecular Technology Research Unit,
School of Science,
Walailak University

PACCON 2011, 7th January 2011

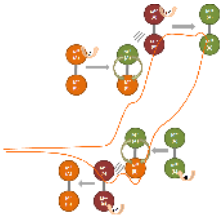

Molecular Technology Research Unit

This presentation focuses on communication between two metal centres in $[(\beta\text{-dkt})_2M(\mu\text{-L})M(\beta\text{-dkt})_2]$ complexes

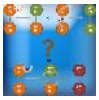

What is redox communication?

What system are we using?

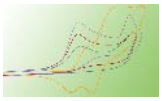

Results and Discussion

2

What is redox communication?

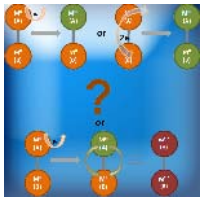

Electronic interaction between two or more redox centres.
The change in oxidation state of one redox centre will induce the electron transfer process across the linker hence the oxidation state of the next redox centre will be changed.

3

Common types of redox communication

Valence-trapped systems:
No electronic interaction between the two redox centres.

- ΔE^0 is small *ca.* 36 mV at 298 K

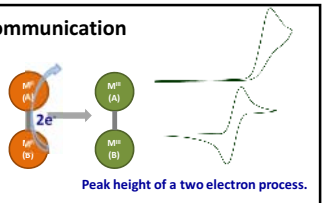

Peak height of a two electron process.

Valence-delocalized system:
Complete charge delocalization over the two redox centres.

- ΔE^0 is large *ca.* 600-700 mV at 298 K

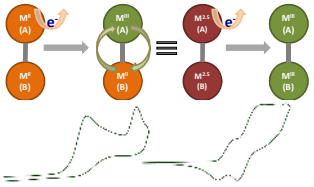

Two well-resolved peaks each corresponding to one electron.

4

Applications of redox communication

Redox switches

Molecular electronic devices (Nano wires)

Molecular magnets

Rewritable molecular memory devices and image processing

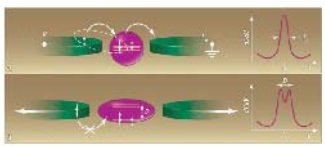

5

What system are we using?

Previous discovery monomeric MO_4N_2 show redox activity.

SCO complexes induced by redox process in Co cases.

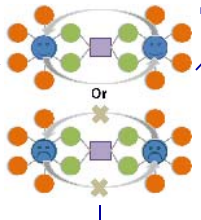

Length and electron density on the linker control the degree of communication.

6

How to design the system?

Co(II): d^7 or Ni(II): d^8

Monomers show redox activity

Spin state depends on the oxidation state and environment

β-diketonate

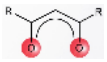

Oxygen donor:

Easy to change the substituent groups

Diimine linkers

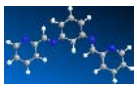

Two nitrogen donor sites:

Easy to modify the length and electron density

Redox process

Cheap and simple technique

Different oxidation states different redox potentials

7

Synthesis of $[(\beta\text{-dkt})_2M(\mu\text{-L})M(\beta\text{-dkt})_2]$ Complexes

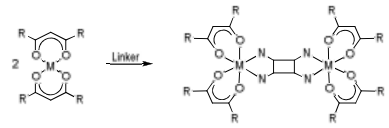

β-diketonate

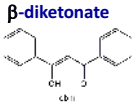

Bridging ligands

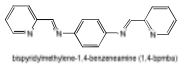

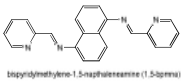

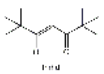

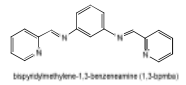

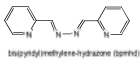

8

Results and Discussion

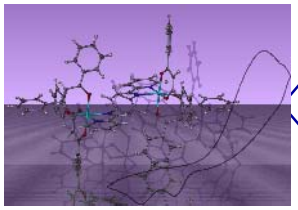

Characterization of $[(\beta\text{-dkt})_2M(\mu\text{-L})M(\beta\text{-dkt})_2]$

Cyclic voltammetry-a way to prove communication

9

Characterization of $[(\beta\text{-dkt})_2M(\mu\text{-L})M(\beta\text{-dkt})_2]$

IR spectroscopic data

The C=O stretches between 1592-1594 cm^{-1} for *dbm* complexes.

The C=O stretch for *tmhd complexes* is *ca.* 5-10 cm^{-1} lower than that of *dbm complexes*

The imine stretches of coordinated bridging ligands *ca.* 1600 and 1630 cm^{-1} are not observed as they masked by the strong C=O stretch of the β-diketonate ligand.

10

X-ray structure of of $[(\beta\text{-dkt})_2M(\mu\text{-L})M(\beta\text{-dkt})_2]$

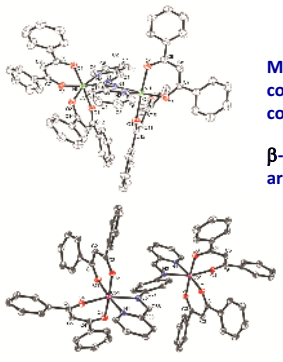

Metal centre is octahedrally coordinated with an O_4N_2 coordination environment

β-diketonate ligands adopt a *cis*-arrangement

11

Cyclic Voltammetric Studies of $[(\beta\text{-dbm})_2Ni(\mu\text{-L})Ni(\beta\text{-dbm})_2]$

L	Peak potential (V)			ΔE (mV) (Ep_2-Ep_1)
	Ep_1	Ep_2	Ep_3	
1,3-bpmba	1.26 (I)	1.54(I)	-	280
1,4-bpmba	1.24 (I)	1.61(I)	-	370
1,5-bpmna	1.32 (I)	1.68(I)	-	360
bpmhd	1.32(I)	1.40(I)	1.64(I)	320*

*Ep_3-Ep_1

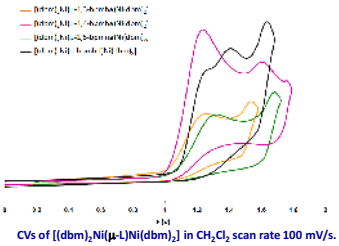

12

CVs of $[(dbm)_2Ni(\mu\text{-L})Ni(dbm)_2]$ in CH_2Cl_2 scan rate 100 mV/s.

Cyclic Voltammetric Studies of $[(\beta\text{-tmhd})_2Ni(\mu\text{-L})Ni(\beta\text{-tmhd})_2]$

L	Peak potential (V)			ΔE (mV) (Ep_2-Ep_1)
	Ep_1	Ep_2	Ep_3	
1,3-bpmba	0.96 (I)	1.54(I)	-	580
1,4-bpmba	1 03(I)	1.51 (I)	-	480
1,5-bpmna	0.94 (I)	1.54(I)	-	600
bpmhd	0.98*	1.23*	1.62(I)	640**

* $E_{1/2}$ for reversible process
**Ep_3-Ep_1

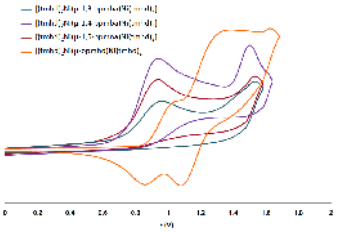

CVs of $[(tmhd)_2Ni(\mu\text{-L})Ni(tmhd)_2]$ in CH_2Cl_2 scan rate 100 mV/s.

13

What's CV telling us?

Mirrors the trend observed in the $[Ni(\beta\text{-dkt})_2(ppa^X)]$ series, the oxidation potential of *dbm* complexes is higher than that of *tmhd* complexes.

The separation between the first and second oxidation peaks is more than 36 mV and peaks height are one electron process. Therefore, there is communication between two Ni centres.

tmhd complexes show better communication between two metal centres.

bpmhd bridged complexes show 3 oxidation peaks and indicate rapid communication between the two metal centres.

14

What is going on in $[(\beta\text{-dkt})_2Ni(\mu\text{-bpmhd})Ni(\beta\text{-dkt})_2]$?

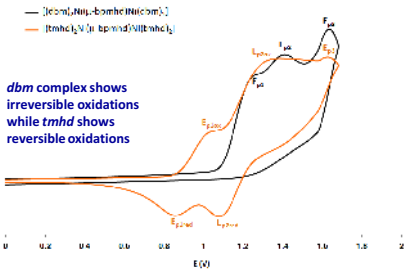

dbm complex shows irreversible oxidations while *tmhd* shows reversible oxidations

There is a third oxidation peak in both complexes. The extra oxidation peak is due to rapid communication between the metal centres over scan rate.

15

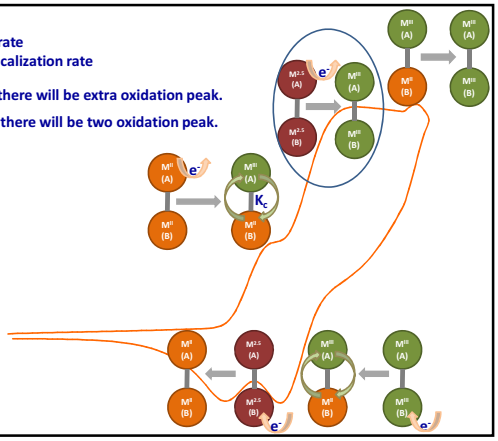

16

Vary scan rate: $[(\beta\text{-dbm})_2Ni(\mu\text{-bpmhd})Ni(\beta\text{-dbm})_2]$

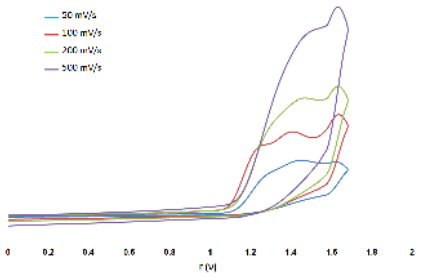

Faster scan rate less well resolved 1st and 2nd oxidation peaks.

17

Cyclic Voltammetric Studies of $[(\beta\text{-dkt})_2Co(\mu\text{-L})Co(\beta\text{-dkt})_2]$

Two oxidation peaks are observed as with the Ni analogous.

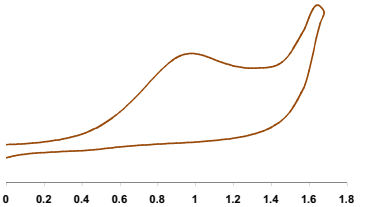

CV of $[(dbm)_2Co(\mu\text{-}1,4\text{-bpmba})Co(dbm)_2]$ in CH_2Cl_2 scan rate 100 mV/s.

However, we are looking for the unusual redox behaviour "*redox induced spin crossover*" in the system so we focus on the 1st oxidation.

18

Redox induced spin crossover in [Co(β-diketonate)$_2$(N-N)]

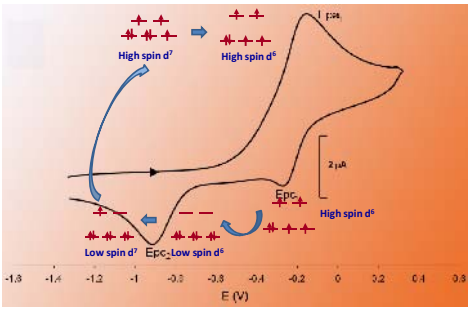

CV of [Co(tmhd)$_2$(phen)] in CH_2Cl_2 scan rate 100 mV/s

19

Cyclic Voltammetric Studies of [(β-dbm)$_2$Co(μ-L)Co(β-dbm)$_2$]

L	Peak potential (V)			ΔE (mV) (Ep$_1$-Ep$_3$)	
	Ep$_1$	Ep$_2$	Ep$_3$		
1,3-bpmba	0.92	-0.18	-	1100	
1,4-bpmba	1.02	-0.14	-	1160	
1,5-bpmna	0.88	0.04	-	920	
bpmhd	1.16	0.22	-0.12	1280*	*Ep$_1$-Ep$_3$

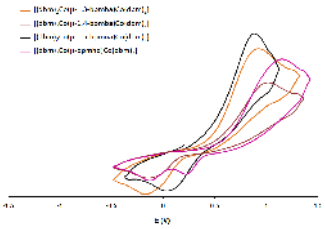

20

CVs of [(dbm)$_2$Co(μ-L)Co(dbm)$_2$] in CH_2Cl_2 scan rate 100 mV/s.

Cyclic Voltammetric Studies of [(β-tmhd)$_2$Co(μ-L)Co(β-tmhd)$_2$]

L	Peak potential (V)			ΔE (mV) (Ep$_1$-Ep$_3$)	
	Ep$_1$	Ep$_2$	Ep$_3$		
1,3-bpmba	1.16	-0.72	-0.96	2160	
1,4-bpmba	0.66	-0.28	-0.42	1080	
1,5-bpmna	0.70	-0.38	-	1080*	*Ep$_1$-Ep$_2$
bpmhd	1.28	0.14	-0.32	1600	

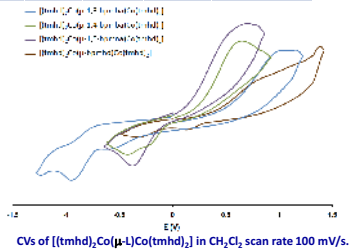

21

CVs of [(tmhd)$_2$Co(μ-L)Co(tmhd)$_2$] in CH_2Cl_2 scan rate 100 mV/s.

What's CV telling us?

The unusual redox behaviour appears to be the result of a spin change upon oxidation – an example of a '*redox induced spin crossover*' as found in the [Co(β-dkt)$_2$(N-N)] complexes.

Most of *tmhd* dimer complexes show two reduction peaks which indicate communication between the two metal centres.

Complication of '*redox induced spin crossover*' effect and metal communication therefore difficult to conclude only from CV studies.

22

In summary, we have synthesized and characterized redox active Ni(II) and Co(II) dimeric complexes which have potential to be the precursors for nanowires.

Further studies on electron communication rate by vary temperature CV, DPV *etc.*

⇩

Computer calculations.

⇩

Adjust the linker to fine tune communication.

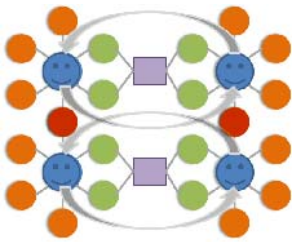

23

Molecular Technology Research Unit

Acknowledgements

Thailand Research Fund and Walialak University (Grant No. RSA5080007)

Molecular Technology Research Unit

Research Team for this work

Assoc. Prof. Dr. David Harding

24

Questions?

Appendix Six

Oral presentation at the Pure and Applied Chemistry International Conference (PACCON2010)

Redox Coupled-Spin Crossover in $[Co(\beta\text{-diketonate})_2(N\text{-}N)]^{0/+}$ Complexes

Phimphaka Harding

Molecular Technology Research Unit,
School of Science,
Walailak University

21st January 2010

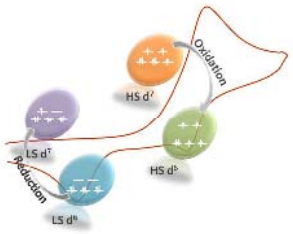

Molecular Technology Research Unit

This presentation focuses on redox coupled-spin crossover (RCSOC) in CoO_4N_2 complexes

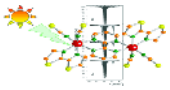

What is spin crossover (SCO)?

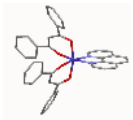

What is our system?

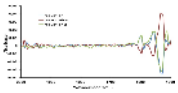

Results and Discussion

2

What is spin crossover (SCO)?

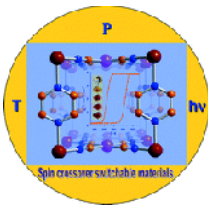

Spin-crossover is the process of changing the spin state of a molecule caused by external constraints (temperature, pressure, or electromagnetic radiation), which induce structural changes at molecular and lattice levels.

3

Common SCO examples

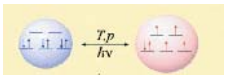

The most common SCO compounds are Fe(II) complexes.

Thermal is the most common external trigger.

Lately, increasing number of complexes have been controlled by light.

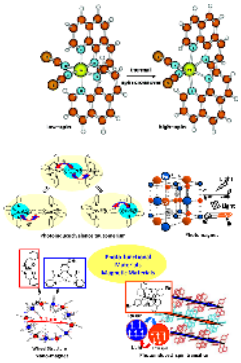

4

Applications of SCO Comlexes

Sensors

Molecular separators of gases

Photonic devices

Light modulators and filters

Rewritable molecular memory devices and image processing

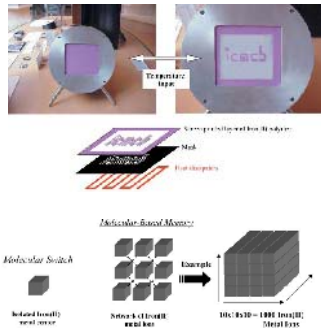

5

What is our system?

Rare SCO Co complexes: CoN_6 $[Co(terpy)_2]^{2+}$ and $[Co(bpy)_3]^{2+}$

Previous discovery NiO_4N_2 show redox activity.

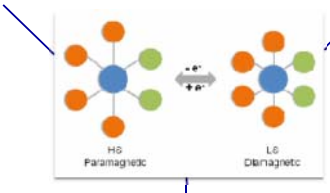

SCO complexes induce by redox process.

6

How to design the system?

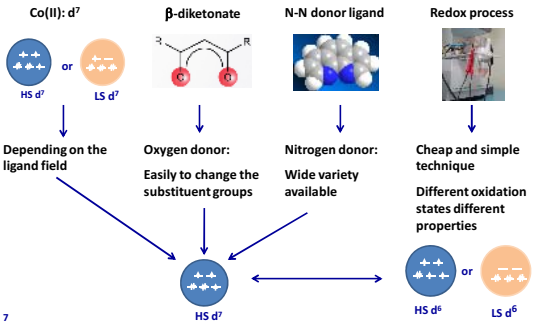

7

Synthesis of [Co(β-diketonate)$_2$(N-N)] Complexes

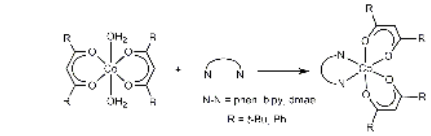

β-diketonate

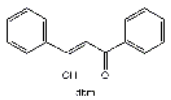

dbm

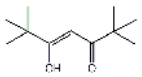

tmhd

N-N donor ligands

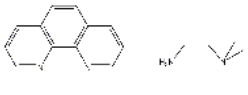

8

Results and Discussion

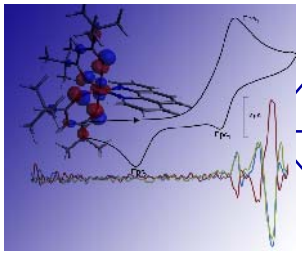

Characterization of [Co(β-diketonate)(N-N)]$^{0/+}$

Cyclic voltammetry-a new discovery!

Spectroelectrochemistry and DFT calculations

9

Characterization of [Co(β-diketonate)$_2$(N-N)]

IR spectroscopic data

C=O stretches between 1550-1600 cm^{-1} suggest symmetrically bound β-diketonate ligands

C-H stretches around 2955 cm^{-1} for tmhd ligands

UV-Vis spectroscopic data

Very strong bands at UV region consistent with ligand centred π-π* transitions

Low intensity d-d transitions were observed around 560 nm

10

X-ray structure of [Co(dbm)$_2$(phen)]

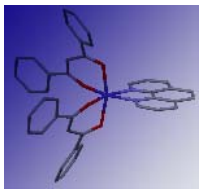

Cobalt metal centre is an octahedrally coordinated with an O_4N_2 coordination environment

β-diketonate ligands adopt a *cis*-arrangement

11

Cyclic Voltammetric Study of [Co(β-diketonate)$_2$(N-N)]

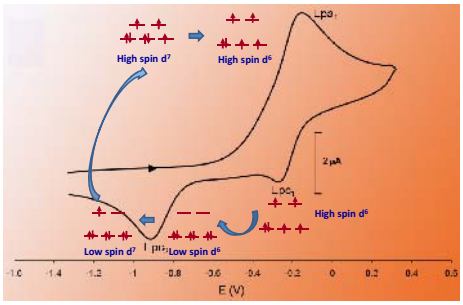

CV of [Co(tmhd)$_2$(phen)] in CH_2Cl_2 scan rate 100 mV/s

12

Fast Scan Cyclic Voltammetry

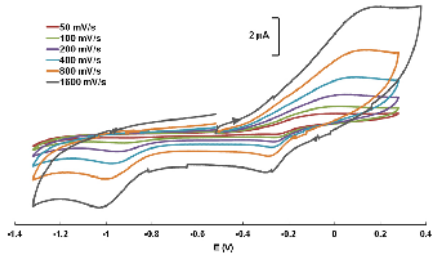

Small change in reversibility at fast scan rate indicate a rapid spin exchange equilibrium and slow electron transfer.

13

What's CV telling us?

The unusual redox behaviour appears to be the result of a spin change upon oxidation – an example of a *'redox induced spin crossover'.*

The oxidation potentials from the CVs indicate that it may be possible to oxidize the Co(II) complexes chemically.

14

Isolation of $[Co(\beta\text{-diketonate})_2(N\text{-}N)]^+$

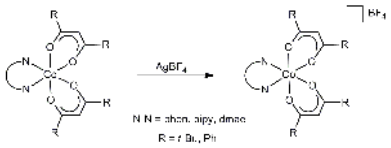

IR spectroscopy: $\nu_{C=O}$ (*ca.* 1550-1520 cm^{-1}) moves to lower wavenumbers compared with the neutral complexes.

The complexes are NMR active indicative of low spin d^6.

15

Cyclic Voltammetric Studies of $[Co(\beta\text{-diketonate})_2(N\text{-}N)]^+$

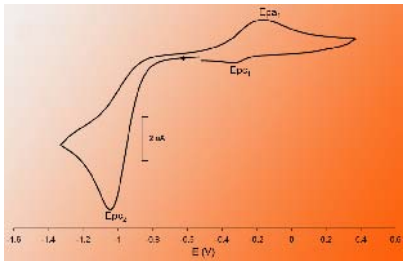

CV of $[Co(tmhd)_2(phen)][BF_4]$ in CH_2Cl_2 scan rate 100 mV/s

16

IR Spectroelectrochemical Studies (SCE)

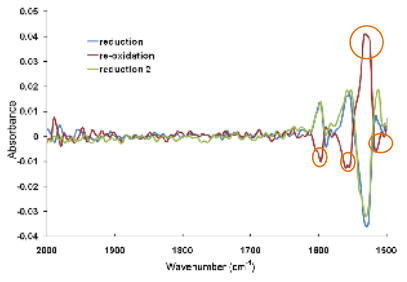

IR spectroelectrochemical difference spectra of $[Co(dbm)_2(phen)][BF_4]$

Loss of $\nu_{C=O}$ at *ca.* 1590, 1570, 1520, 1500 cm^{-1} due to Co(II) starting material.

Increasing of $\nu_{C=O}$ at *ca.* 1550 and 1520 cm^{-1} due to Co(III) product.

17

DFT of $[Co(\beta\text{-diketonate})_2(N\text{-}N)]^{0/+}$

B3LYP/SDD calculations confirm HS state is most stable for Co(II) and LS state for the Co(III) complexes.

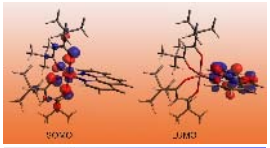

SOMO is composed of an antibonding interaction between β-diketonate oxygen *p*-orbitals and the Co d_{z^2} orbital for all *tmhd* complexes and $[Co(dbm)_2(dmae)]$.

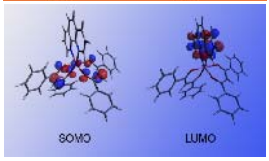

SOMO for other *dbm* complexes is composed of a weaker antibonding interaction between β-diketonate and the Co d_{xz} orbital

18

DFT Calculations & Electrochemical Studies

Complex	E(HS)-E(LS)/(kcal.mol^{-1})
[Co(tmhd)$_2$(phen)]	-15.63
[Co(tmhd)$_2$(2,2′-bpy)]	-14.55
[Co(tmhd)$_2$(dmae)]	-12.67
[Co(dbm)$_2$(phen)]	-13.84
[Co(dbm)$_2$(2,2′-bpy)]	-12.80
[Co(dbm)$_2$(dmae)]	-13.26
[Co(tmhd)$_2$(phen)]$^+$	16.12 (16.38)
[Co(tmhd)$_2$(2,2′-bpy)]$^+$	17.15 (17.19)
[Co(tmhd)$_2$(dmae)]$^+$	17.41 (17.60)
[Co(dbm)$_2$(phen)]$^+$	16.93 (17.31)
[Co(dbm)$_2$(2,2′-bpy)]$^+$	18.01 (18.16)
[Co(dbm)$_2$(dmae)]$^+$	17.93 (16.61)

ΔE(HS-LS) is small

Observed the HS d^6 intermediate in electrochemical studies

19

In summary, we have synthesized and characterized the redox coupled-spin crossover $Co^{2+/3+}$ complexes which have potential to be nano-switches.

Require low applied potential to induce SCO behaviour

⬇

Easy to fine tune by changing coordination environments

⬇

Extendable to multifunctionallized materials

20 Molecular Technology Research Unit

Acknowledgements

Thailand Research Fund and Walialak University (Grant No. RSA5080007)

Molecular Technology Research Unit

Research Team for this work

Assoc. Prof. Dr. David Harding

Asst. Prof. Dr. Yuthana Tantirungrotechai, National Nanotechnology Centre, Thailand

Theeraphol Thurakitsaree

Rattawat Daenggern

Prof. Dr. Mike Shaw and Brian Schutte, SIUE, USA

21

Questions?

22 Molecular Technology Research Unit

Appendix Seven

Oral presentation at The 8th Conference of the Inorganic Chemistry Division (IC08)

Electron Transfer of Co(II) and Ni(II) ß-Diketonate Complexes Incorporating Asymetric Diimine Ligands

Dr. Phimphaka Harding
Molecular Technology Research Unit
Walailak University

Introduction

- Aims
  - To study the electrochemical properties of metal β-diketonate complexes.
  - Fine tune the redox properties by varying the groups on the β-diketonate and diimine ligands.
- Background
  - Only a few β-diketonates studied.
  - Most diimines have been symmetric.
  - Virtually no electrochemical studies have been reported.

Ref:
1. P. Harding, D.J. Harding, W. Phonsri, S. Saithong and H. Phetmung, *Inorg. Chim. Acta*, 2009, 1, 78.
2. P. Chassot and F. Emmenegger, *Inorg. Chem.*, 1996, 35, 5931.

What is a Metal β-Diketonate?

- Metal β-diketonate complexes, $[M(\beta\text{-diketonate})_2]$ (M = Ni, Co, Fe, Cu *etc.*)
- Stable in air.
- Easy to make.
- Dissolve in organic solvents.
- Applications in catalysis, magnetic, electronic and optical devices.
- *Cis* and *trans* isomers are frequently encountered.

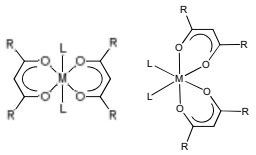

What do we use in this work?

- $[M(\beta\text{-diketonate})_2(H_2O)_2]$ when M = Ni and Co, β-diketonate ligands = dbm, tmhd and hfac.

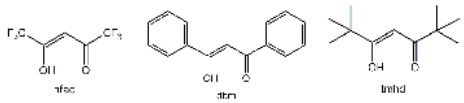

- (4-X-phenyl)-pyridin-2-ylmethylene-amine (ppa^X).

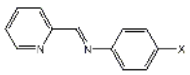

How to make Metal β-Diketonates?

- Reaction of β-diketonates with a metal acetate gives $[M(\beta\text{-diketonate})_2(H_2O)_2]$.

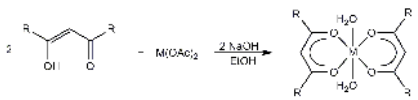

How to make the ppa^X ligands?

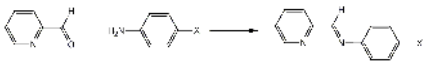

- X = H, Me, Et, OMe, F, Cl, Br and I.
- Molecular sieves are necessary to absorb water to allow isolation of the ppa^X ligands.

Ref:
1. S. Dehghanpour and A. Mahmoudi, *Main Group Chemistry*, 2007, 6, 121.
2. S. Dehghanpour, N. Bouslimani, R. Welter and F. Mojahed, *Polyhedron*, 2007, 26, 154.

Synthesis of [M(β-diketonate)$_2$ (ppa^x)] Complexes

- Simple addition of the ppa^X ligand to a solution of the metal β-diketonate yields the target compounds.

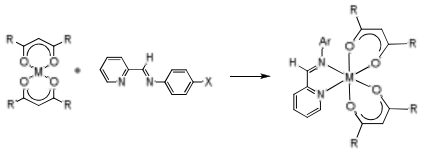

Characterization of Metal Complexes

Ni Complexes

- IR spectroscopy indicates chelating β-diketonate ligands ($\nu_{C=O}$ = 1588-1595 cm^{-1} for *dbm* and *tmhd* and 1647-1654 cm^{-1} for *hfac*).
- UV-Vis spectroscopy:

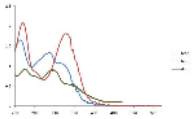

UV-Vis spectra of [Ni(β-diketonate)$_2$(ppa^{OMe})].

Co Complexes

- IR spectroscopy: $\nu_{C=O}$ = 1586-1596 cm^{-1} for *dbm* and *tmhd* complexes and 1646-1649 cm^{-1} for *hfac* complexes.
- UV-Vis spectroscopy:

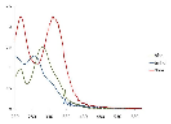

UV-Vis spectra of [Co(β-diketonate)$_2$(ppa^{OMe})].

X-ray Structures of Co and Ni Complexes

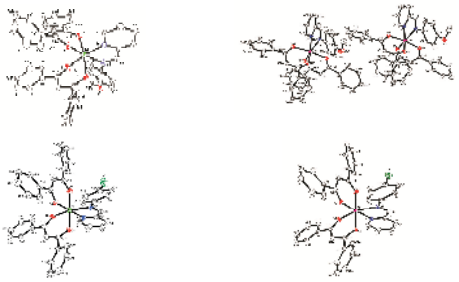

X-ray Structures of Co and Ni Complexes

- The *dbm* ligands exhibit both 'planar' and 'bent' coordination modes.

	Ni-ppa^{Cl}	Ni-ppa^{Me}	Ni-ppa^{OMe}	Co-ppa^{OMe}
M-N1	2.091(2)	2.090(4)	2.0812(14)	2.1408(14)
M-N2	2.189(2)	2.180(4)	2.1096(14)	2.1951(14)
M-O1	2.0091(16)	2.013(3)	2.0349(12)	2.0769(12)
M-O2	2.0205(17)	2.005(3)	2.0135(12)	2.0260(12)
M-O3	2.0165(16)	2.027(3)	2.0479(12)	2.0988(11)
M-O4	2.0128(16)	2.010(4)	2.0163(12)	2.0450(12)
β	2.98, 17.06	1.51, 16.57	31.94, 24.72	15.62, 21.94

Crystal Packing in [M(β-diketonate)$_2$ (ppa^x)] Complexes

[Ni(dbm)$_2$(ppa^{Cl})] **[Ni(dbm)$_2$(ppa^{OMe})]**

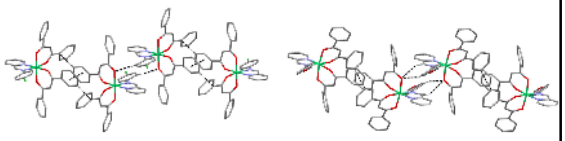

- The complexes are packed in chiral columns.
- CH…O interactions exist between the ppa^X and dbm ligands.
- For X = Cl, Me π…π and CH…π interactions are also observed.

Electron Transfer Studies of Ni Complexes

- Redox processes for the Ni complexes depend on the substituent groups of the β-diketonate ligands.
- The X group on the ppa^X ligands has only a small effect on the redox potential.
- When X is a halide an additional reduction wave is observed.

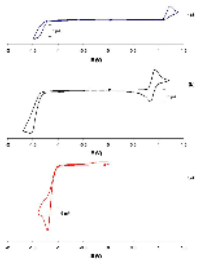

CVs of (a) [Ni(dbm)$_2$(ppa^F)], (b) [Ni(tmhd)$_2$(ppa^F)], (c) [Ni(hfac)$_2$(ppa^F)].

Electron Transfer Studies of Co Complexes

- In contrast to the Ni analogues the Co complexes show unexpected behaviour upon oxidation.
- In theory Co(III) is normally more stable than Ni(III).

Why do we observe an irreversible oxidation for the dbm and tmhd complexes?

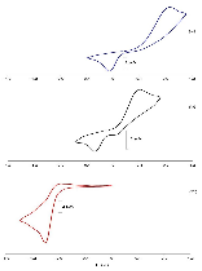

CVs of (a) [Co(dbm)$_2$(ppa^{Cl})], (b) [Co(tmhd)$_2$(ppa^{Cl})], (c) [Co(hfac)$_2$(ppa^{Cl})].

Electron Spin Change upon Oxidation

- The unusual redox behaviour appears to be the result of a spin change upon oxidation – an example of a '*redox induced spin crossover*'.

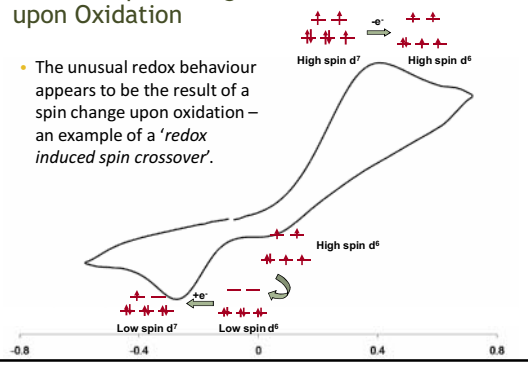

Electron Transfer Studies of Co Complexes

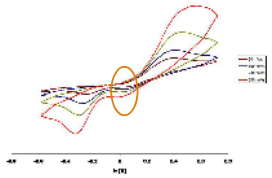

CVs of [Co(tmhd)$_2$(ppa^{Cl})] at different scan rates.

- At higher scan rates the reduction peak for the high spin Co(III) species becomes more visible.
- The stability of the high spin Co(III) species also depends on the nature of the substituent on the β-diketonate ligand.

Isolation of Co(III) Complexes

- The oxidation potentials from the CVs indicate that it may be possible to oxidize the Co(II) complexes chemically.

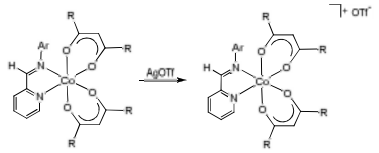

Characterization of Cationic Complexes

- IR spectroscopy: $\nu_{C=O}$ moves to lower wavenumbers compared with the neutral complexes.
- The complexes are NMR active indicative of low spin d^6.

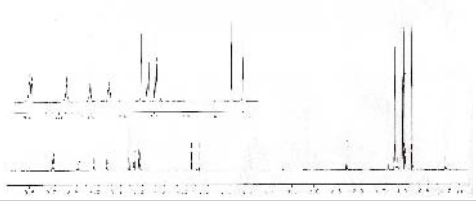

CVs of the Redox Pair

- The oxidation and reduction potentials of the neutral and cationic species are identical.

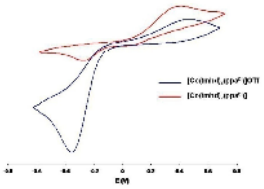

CV of [Co(tmhd)$_2$(ppa^{Cl})] (–) and [Co(tmhd)$_2$(ppa^{Cl})]$^+$ (–).

Acknowledgements

- Thailand Research Fund (TRF)
- Walailak University
- Molecular Technology Research Unit (MTRU)
- University of Sheffield for X-ray structures
- University of Bristol UK for CHN and MS
- Summer training students: Nitisasrt Soponrat, Kittaya Tinpun and Sirirat Samuadnuan
- Assoc. Prof. Dr. David J. Harding

Appendix Eight

Oral presentation at Metrohm Siam Ltd.

Simultaneous UV-Vis Spectroelectrochemistry

Assist. Prof. Dr. Phimphaka Harding
Molecular Design & Electrochemistry Laboratory
Walailak University

URL: http://sites.google.com/site/mdelwu

What is Simultaneous UV-Vis Spectroelectrochemistry

- The spectroelectrochemical technique that couples a UV-Vis spectrometer with an electrochemical apparatus.
- Uses a fiber-optic dip probe to achieve simultaneous results from the electrochemical cell.

1

What's new?

Normal UV-Vis SEC

Picture taken at Prof. Reynolds, University of Florida, USA

Fiber-Optic UV-Vis SEC

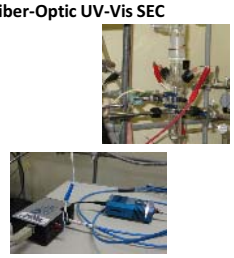

Picture taken at Prof. Mike Shaw, Southern Illinois University of Edwardsville (SIUE), USA

2

What do we need to set-up SEC (as at SIUE)?

- Potentiostat
- Light source
- Detector
- Fiber-optic probes
- Electrochemical cells
- Electrodes
- Labview program
- USB-6251-BNC: interface

3

Fiber-Optic Spectroelectrochemical Instrumentation Scheme

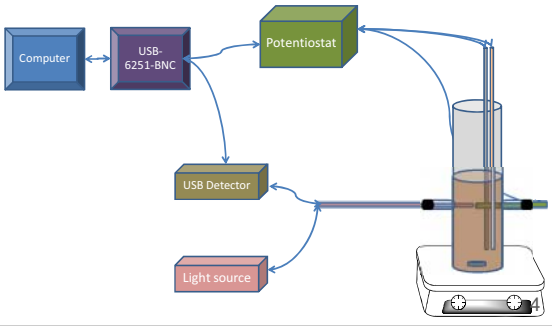

4

Step by Step Simultaneous UV-Vis Spectroelectrochemistry

Find the working electrode area (only one time for new electrode)

Find the diffusion coefficient of compound

Study Beer's Law Plot

Run Simultaneous UV-Vis Spectroelectrochemistry

5

Finding the working electrode area

- Prepare the mixed solution of $K_4[Fe(CN)_6]$ 1 mM and KCl 0.1 M in water.
- Using 3.0 mm Pt as working electrode, Pt wire as Aux. and Ag wire as Ref.
- Run Chronoamperometry at room temperature.

$$I = \frac{nFAD^{1/2}C_0}{\pi^{1/2}t^{1/2}}$$

Diffusion coefficient of $K_4[Fe(CN)_6]$ in 0.1 M KCl at 25 °C = 0.65 x 10^{-5} cm^2/s

Note: We need to do this only for first time!!

6

Instrumentation Scheme for Chronoamperometry (CA)

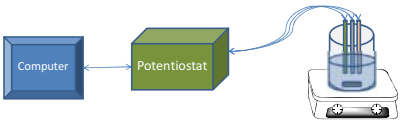

7

Program for Chronoamperometry Experiment

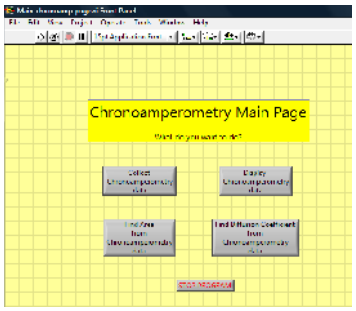

8

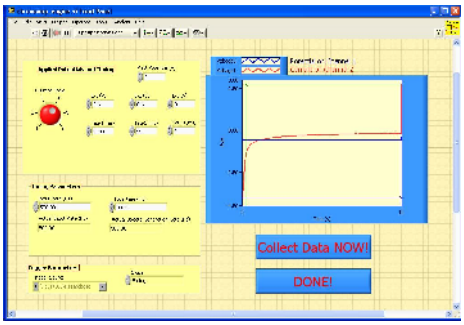

9

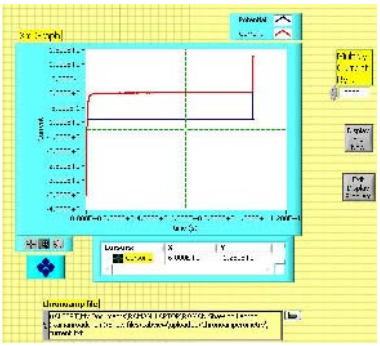

10

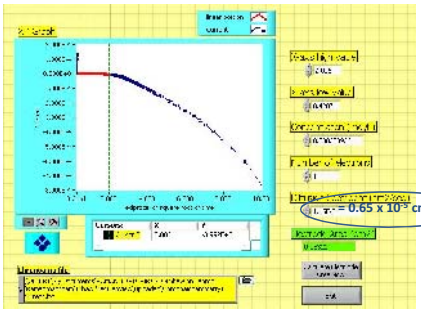

11

Finding the Diffusion Coefficient

- Prepare 1mM solution of the compound and $[NBu_4][PF_6]$ 0.1 M in 10 mL CH_2Cl_2
- Using 3.0 mm Pt as working electrode, Pt wire as an Aux. electrode and Ag wire as a Ref. electrode.
- Run Chronoamperometry at room temperature.
- Find the compound's Diffusion Coefficient.

12

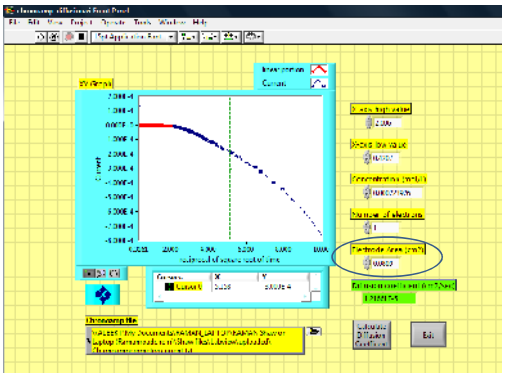

13

Beer's Law Plots Instrumentation Scheme

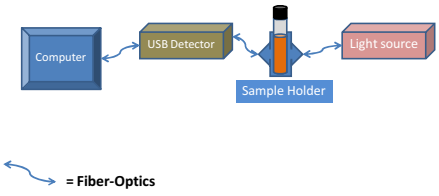

= Fiber-Optics

14

Beer's Law Plot

Experimental

- Prepare a stock solution of compound such as 0.5 mM.
- Make dilute solutions *e.g.* 0.1, 0.2, 0.3 and 0.4 mM.
- Measure the absorptions.
- Plot graph A vs. Conc.

15

Simultaneous UV-Vis SEC

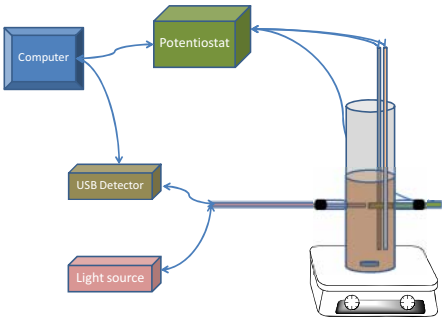

16

What do we do next?

- Firstly, apply a constant potential that will reduce or oxidize the compound.
- Then measure and collect the spectra of the species at the working electrode surface every 0.5 seconds, 20 times

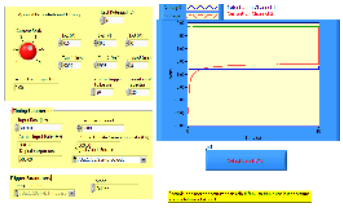

17

Principles of the experiment set-up

- The UV-Vis beam is focused from the spectrometer into a set of UV-Vis optical fibers.
- The beam exits the fibers through the probe assembly, travels through the reaction solution, bounces of the electrode and is collected by another set of fibers which lead to the detector.

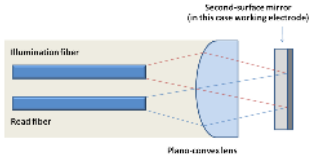

18

Principles of the experiment set-up

- The difference spectra between the bulk solution with no potential applied and spectra where potential has been applied for at least 15 sec. clearly indicate the presence and identity of the thus-formed electrode products.

19

What's going on in the cell

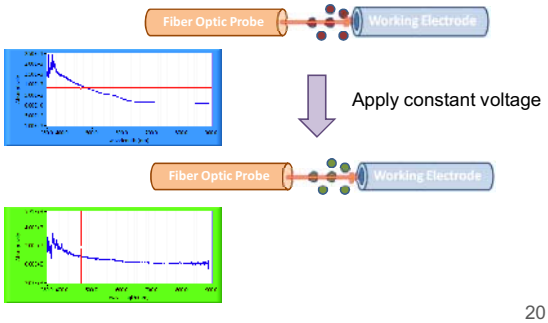

20

Data Manipulation

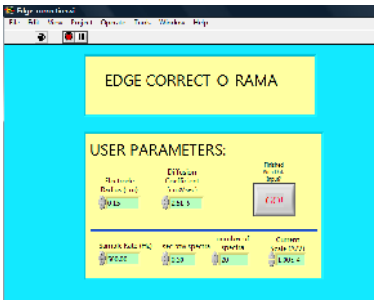

21

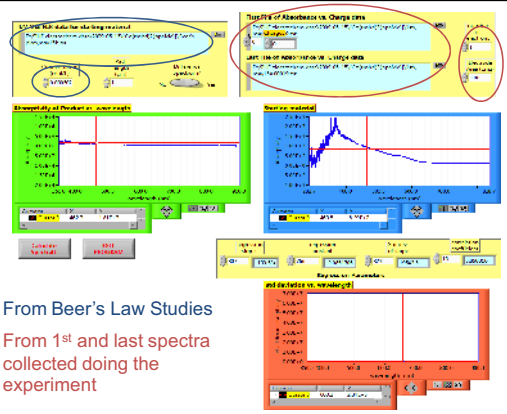

From Beer's Law Studies

From 1st and last spectra collected doing the experiment

22

Why do we need edge correction?

Ideal electrode:
No uneven electrode surface

Real electrode:
There is an edge on the electrode surface. → More reaction surface area than just the area of electrode as we use in the equation.

23

Edge Correction Data

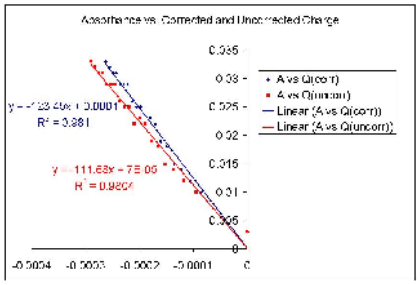

24

Ferrocene UV-Vis spectroelectrochemical spectra

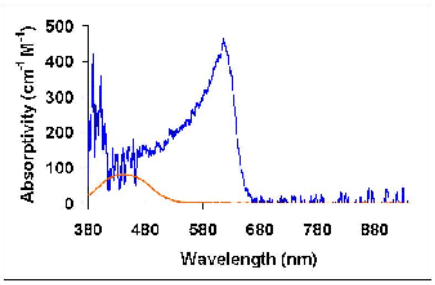

25

Acknowledgements

- UMAP and WU for travelling support to SIUE.
- TRF for research fund.
- Prof. Mike Shaw for access the SEC.
- Assoc. Prof. Dr. David Harding and Benjamin Harding for making life at SIUE more fun.
- Metrohm Siam Ltd. for today's seminar.
- Your attention!

26

Appendix Nine

Poster presentation the Annual Thailand Research Fund, Phetchaburi, Thailand, 2010

Redox Coupled-Spin Crossover Cobalt β-Diketonate Complexes: Synthesis, Electron Transfer Studies and DFT Calculations

Harding, P.[1*], Harding, D.J.[1], Tantirungrotechai, Y.[2] and Sayananon A.[3]

[1] Molecular Technology Research Unit, School of Science, Walailak University, Nakhon Si Thammarat, 80161, Thailand

[2] National Nanotechnology Center, National Science and Development Agency, Pathumthani, 12120, Thailand

[3] Department of Chemistry, Faculty of Science, Thammasat University, Pathumthani, 12120, Thailand

URL: http://sites.google.com/site/mdelwu E-mail: kphimpha@wu.ac.th

Objective

- To synthesize novel mononuclear metal complexes [Co(β-dkt^{R})$_2$(ppa^{X})] and their cations.
- To investigate the effect of type of substituent groups on ligands on electron transfer of cobalt β-diketonate complexes.
- To study the electronic properties of [Co(β-dkt^{R})$_2$(ppa^{X})] and their cations by using DFT calculations.
- To study inter- and intramolecular forces in the metal complexes.

Methodology

Ligand Synthesis

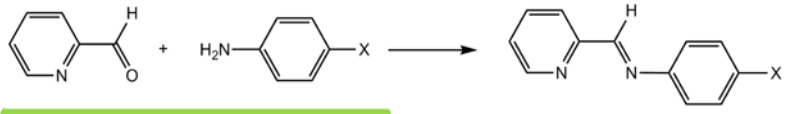

Co(II) Complexes Synthesis

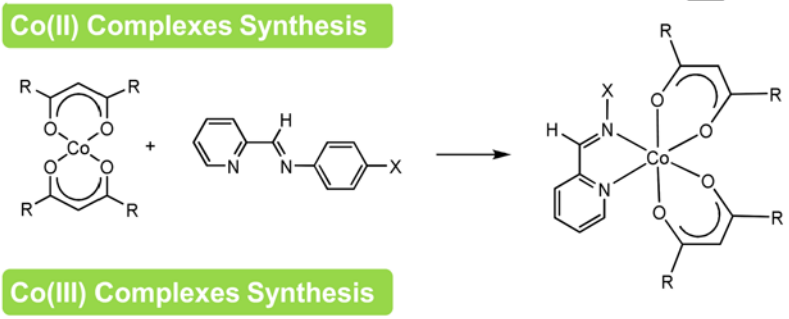

Co(III) Complexes Synthesis

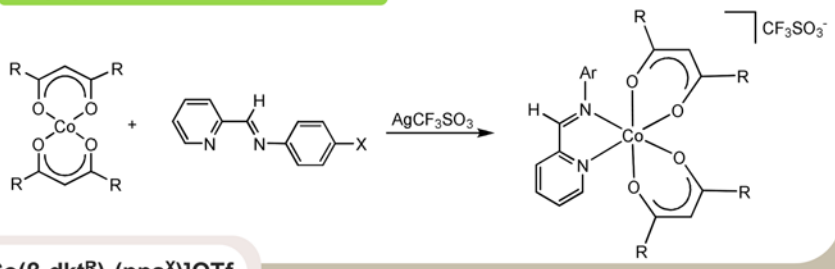

Results and Discussion

Electron Transfer Studies

The [Co(β-dkt^{R})$_2$(ppa^{X})] complexes (β-dkt^{R} = dbm or tmhd) show an irreversible oxidation followed by a reduction of an unknown peak which indicative that upon oxidation there is a change in spin state from high spin to low spin. This behaviour is know as *"redox coupled spin-crossover"*.

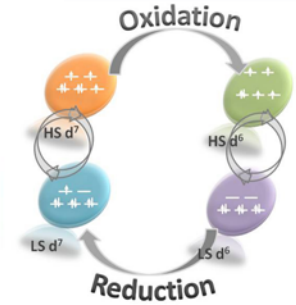

The CV of [Co(β-dkt^{R})$_2$(ppa^{X})]OTf are almost identical to those found in the neutral analogues although there are slight deviations.

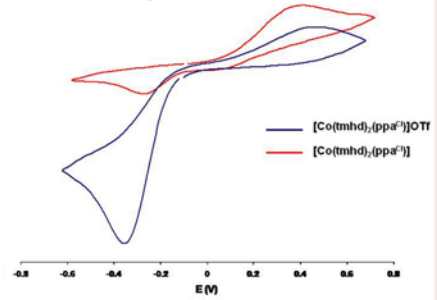

Figure 1 CVs of [Co(tmhd)$_2$(ppa^{Cl})] and [Co(tmhd)$_2$(ppa^{Cl})]OTf

DFT Calculations

DFT calculations of [Co(β-diketonate)$_2$(ppa^{X})] complexes have suggested that SOMO is constituted of Co (*ca.* 40%), β-diketonate (*ca.* 55%) and ppa^{X} (*ca.* 5%) hence the oxidation potential will depend mostly on the properties of substituents on the β-diketonate.

Acknowledgements and Output

Acknowledgements

We thank Walailak University and the Thailand Research Fund for supporting this research (RSA 5080007).

Output

1. P. Harding, D. J. Harding, K. Tinpun, S. Samuadnuan, N. Sophonrat and H. Adams, Synthesis and electrochemical studies of nickel β-diketonate complexes incorporating asymmetric diimine ligands, *Aust. J. Chem*, 2010, 63, 75.
2. P. Harding, D. J. Harding, N. Sophonrat and H. Adams, Bis(1,1,1,5,5,5-hexafluoropentane-2,4-dionato-κ^2-*O*,*O*')[(4-bromo-phenyl)pyridin-2-ylmethyleneamine-κ^2-*N*,*N*']cobalt(II), *Acta Cryst. Section E*, 2010, E66, m1138.

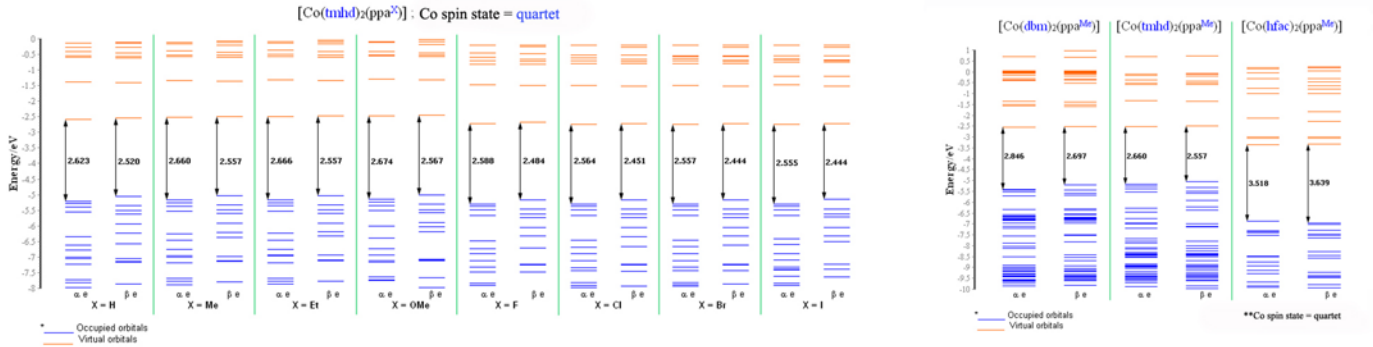

Figure 2 Plot of the SOMO-LUMO gap with the tmhd series showing the effect of the ppa^{X} ligand and the effect of the β-diektonate when the diimine is ppa^{Me}.

Appendix Ten

Poster presentation the Annual Thailand Research Fund, Phetchaburi, Thailand, 2009

Electronic Communication in Redox Coupled-Spin Crossover Cobalt Dimers

Phimphaka Harding* and David J. Harding

Molecular Technology Research Unit, School of Science, Walailak University, Thasala, Nakhon Si Thammarat, 80161, Thailand
E-mail: kphimpha@wu.ac.th URL: http://sites.google.com/site/mdelwu/

Introduction

The Co β-diketonate monomeric complexes *e.g.* [Co(β-diketonate)$_2$(ppa^X)] show redox coupled-spin crossover (RCSC) behaviour. In this work we explored the possibility of modified RCSC behaviour in a Co dimers.

Objectives

- To synthesize [(β-diketonate)$_2$Co(μ-L)Co(β-diketonate)$_2$] complexes.
- To investigate the redox coupled-spin crossover behaivour of the dimeric complexes using cyclic voltammetry.

Synthesis

The reaction of various diamines and pyridine-2-carboxaldehyde yields bispyridylmethylenediamine bridging ligands (Scheme 1).

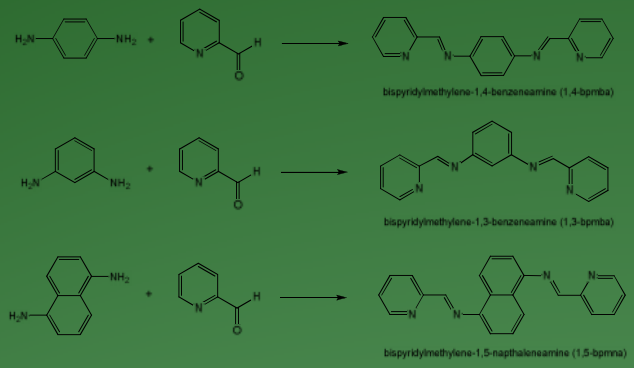

Scheme 1 Ligands synthesis.

The Co dimer complexes were prepared by the reaction of [Co(β-diketonate)$_2$] (β-diketonate = dbm and tmhd) with one equivalent of the bridging ligands (Scheme 2) resulting in formation of the novel Co dimer complexes, [(dbm)$_2$Co(μ-L)Co(dbm)$_2$] (L = 1,3-bpmba **1**, 1,4-bpmba **2** and 1,5-bpmna **3**) and [(tmhd)$_2$Co(μ-L)Co(tmhd)$_2$] (L = 1,3-bpmba **4**, 1,4-bpmba **5** and 1,5-bpmna **6**).

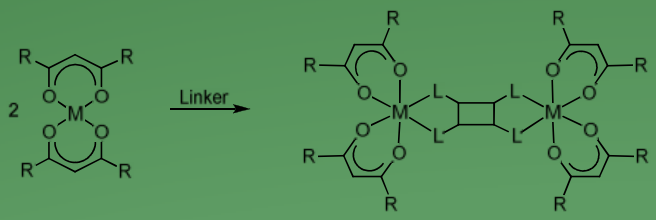

Scheme 2 Co dimers synthesis.

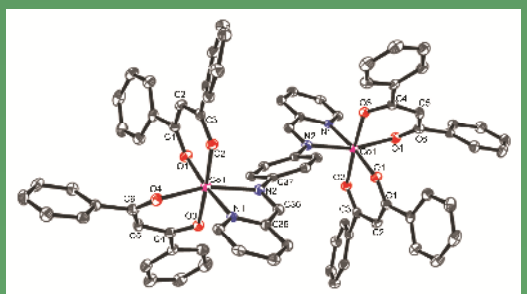

Figure 1 X-ray structure of [(dbm)$_2$Co(μ-1,4-bpmab)Co(dbm)$_2$] **2**.

Electrochemical Studies

The cyclic voltammograms of the Co dimers **1**-**6** show oxidation peaks followed by returned peaks which are separated from the oxidation peaks by *ca.* 800-2000 mV indicative of the RCSC behavior observed in the [Co(β-diketonate)$_2$(ppa^X)] and [Co(β-diketonate)$_2$(N-N)] complexes.

- In the *dbm* series the stabilization ability of the ligands is in the order of *1,4-bpmba > 1,3-bpmba > 1,5-bpmna*. While for the *tmhd* series no trend is observed.

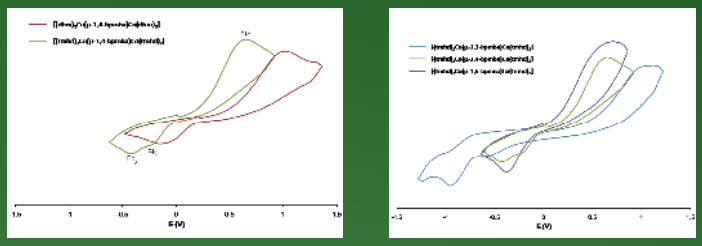

Figure 2 Cyclic voltammograms of Co dimers.

Comparison between the Co-tmhd complexes **4**-**6** found [(tmhd)$_2$Co(μ-1,3-bpmba)Co(tmhd)$_2$] **4** is more difficult to oxidize than the other two complexes by *ca.* 300 mV and also more difficult to oxidize than [(dbm)$_2$Co(μ-1,3-bpmba)Co(dbm)$_2$] **1** by *ca.* 100 mV. This unusual electron transfer behavior and might be due to strong communication between two metal centres through the bridging ligand. It is also possible that the structural reorganization required upon oxidation is more difficult to achieve as a result of increased steric interactions that would be expected in the 1,3-bpmba ligand complexes.

Table 1 Electrochemical data for Co dimers.

Complex	Peak potential (V)		
	Ep_1	Ep_2	Ep_3
[(dbm)$_2$Co(μ-1,3-bpmba)Co(dbm)$_2$] **1**	0.96	-	-0.16
[(dbm)$_2$Co(μ-1,4-bpmba)Co(dbm)$_2$] **2**	1.02	-	-0.14
[(dbm)$_2$Co(μ-1,5-bpmna)Co(dbm)$_2$] **3**	0.88	-	0.04
[(tmhd)$_2$Co(μ-1,3-bpmba)Co(tmhd)$_2$] **4**	1.04	-0.56	-0.96
[(tmhd)$_2$Co(μ-1,4-bpmba)Co(tmhd)$_2$] **5**	0.67	-0.22	-0.42
[(tmhd)$_2$Co(μ-1,5-bpmna)Co(tmhd)$_2$] **6**	0.70	-	-0.38

Acknowledgements

We acknowledge the Thailand Research Fund and Walailak University for research grant number RSA5080007.

Appendix Eleven

Poster presentation the Annual Thailand Research Fund, Phetchaburi, Thailand, 2008

Electron Transfer Studies of [Ni(β-diketonate)$_2$(ppa^X)] Complexes

P. Harding*[1], D.J. Harding[1], N. Sophonrat[2], K. Tinpun[2], S. Samuadnuan[2], H. Adams[3]

[1] Molecular Technology Research Unit, School of Science, Walailak University, Nakhon Si Thammarat, 80161, Thailand

[2] Department of Chemistry, Faculty of Science, Taksin University, Songkhla, 90000, Thailand

[3] Department of Chemistry, University of Sheffield, Brook Hill, Sheffield, S3 7HF, England

Corresponding author e-mail: kphimpha@wu.ac.th URL: http://resource.wu.ac.th/inorganic_synthesis

Introduction

Metal β-diketonate complexes have found many applications but the redox chemistry of these systems is under developed. In this work we synthesize a series of novel Ni(II) β-diketonate complexes incorporating asymmetric diimine ligands, [Ni(β-diketonate)$_2$(ppa^X)]. These complexes have been investigated by cyclic voltammetry to better understand their redox behaviour.

Synthetic Method

The reaction of [Ni(dbm)$_2$], [Ni(tmhd)$_2$] or [Ni(hfac)$_2$] with eight (4-X-phenyl)-pyridin-2-ylmethylene-amine ligands, ppa^X, when X = H **1**, Me **2**, Et **3**, OMe **4**, F **5**, Cl **6**, Br **7** and I **8** in CH_2Cl_2 , THF or acetone affords yellow, red or orange solids of the octahedral complexes, [Ni(dbm)$_2$(ppa^X)] (X = H **9**, Me **10**, Et **11**, OMe **12**, F **13**, Cl **14**, Br **15** and I **16**), [Ni(tmhd)$_2$(ppa^X)] (X = H **17**, Me **18**, Et **19**, OMe **20**, F **21**, Cl **22**, Br **23** and I **24**), [Ni(hfac)$_2$(ppa^X)] (X = H **25**, Me **26**, Et **27**, OMe **28**, F **29**, Cl **30**, Br **31** and I **32**). (Scheme 1)

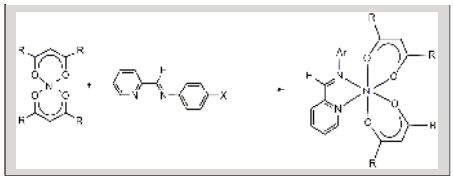

Scheme 1 *Synthesis of [Ni(β-diketonate)$_2$(ppa^X)] complexes.*

Results and Discussion

Molecular structure of complexes **10**, **12** and **14** were determined by X-ray crystallography. The structure of **10** is shown in Figure 1. Complexes **10**, **12** and **14** assume slightly distorted octahedral coordination geometries. The β-diketonate ligands exhibit a *cis* arrangement enforced by the chelating ppa^X ligand.

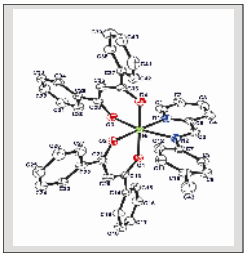

Figure 1 *Molecular structure of [Ni(dbm)$_2$(ppa^{Me})] **10**.*

The redox chemistry of complexes **9**-**32** were studied by cyclic voltammetry in CH_2Cl_2 at room temperature (Table 1).

Table 1 *Electrochemical data of [Ni(β-diketonate)$_2$(ppa^X)] complexes.*

Complex	E_{ox} (V)	E_p^{red} (V)	Complex	E_{ox} (V)	E_p^{red} (V)
9	1.19 (I)	-	**21**	0.87	-1.57 (I)
10	1.18 (I)	-	**22**	0.87	-1.49 (I)
11	1.18 (I)	-	**23**	0.88	-1.46 (I)
12	1.18 (I)	-	**24**	0.89	-1.48 (I)
13	1.20 (I)	-1.42 (I)	**25**	-	-1.24 (I)
14	1.24 (I)	-1.32 (I)	**26**	-	-1.27 (I)
15	1.20 (I)	-1.33 (I)	**27**	-	-1.17 (I)
16	1.22 (I)	-1.31 (I)	**28**	-	-1.22 (I)
17	0.85	-	**29**	-	-1.21 (I)
18	0.84	-	**30**	-	-1.05 (I)
19	0.83	-	**31**	-	-1.09 (I)
20	0.84, 1.49(I)	-	**32**	1.10 (I)	-1.09 (I)

[a] All measurements were performed at 298 K, in dried and degassed CH_2Cl_2 0.1 M [NBu$^n_4$][PF$_6$] solution; scan rate 100 mVs^{-1}; calibrated with [Fe(η-C$_5$H$_5$)$_2$], $E^{o'} = 0.52$ V. [b] E_{ox} represents $E^{o'}$ if the oxidation is reversible and the peak potential, E_p^{ox}, if the oxidation is irreversible. [c] Uncalibrated as the compound reacts with [Fe(η-C$_5$H$_5$)$_2$].

The results show that changing the substitutents on the β-diketonate ligands plays a more important role in the electron transfer behaviour than that of the ppa^X ligand. The increase in electron donating ability from hfac to tmhd and the corresponding change in redox-behaviour from no oxidation to irreversible oxidation to quasi-reversible oxidation, in the case of hfac, dbm and tmhd respectively (Figure 2). Moreover, when the substitutent on the ppa^X is a halide, the complexes undergo an irreversible reduction in all cases.

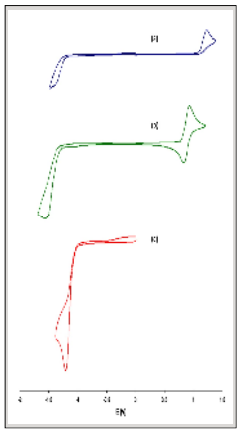

Figure 2 *Cyclic voltammograms of (a) [Ni(dbm)$_2$(ppa^F)], **13** (b) [Ni(tmhd)$_2$(ppa^F)], **21** (c) [Ni(hfac)$_2$(ppa^F)] **29**.*

Conclusion

The electron transfer behaviour of Ni(II) complexes, [Ni(β-diketonate)$_2$(ppa^X)], are irreversibly or reversibly oxidised to Ni(III) in the case of [Ni(dbm)$_2$(ppa^X)] and [Ni(tmhd)$_2$(ppa^X)], respectively. With the exception of [Ni(hfac)$_2$(ppa^I)] which show no oxidation processes. The β-diketonate ligand has a significant effect on the redox potential while the ppa^X ligands have only a very minor effect.

References

1. P. Harding, D. J. Harding, W. Phonsri, S. Saithong, H. Phetmung, *Inorg. Chim. Acta.*, **2008**, DOI:10.1016/j.ica.2008.03.014.
2. P. Chassot and F. Emmenegger, *Inorg. Chem.*, 1996, **35**, 5931-5934.
3. D. V. Soldatov, I. L. Moudrakovski, C. I. Ratcliffe, R. Dutrisac and J. A. Ripmeester, *Chem. Mater.*, 2003.

Acknowledgements

We would like to thank the Thailand Research Fund (TRF) and Walailak University for financial support (RSA-5080007).